

This document is the accepted manuscript version of the following article:

Bröde, P., Aerts, J. M., De Bruyne, G., Mayor, T. S., Annaheim, S., Fiala, D., & Kuklane, K. (2023). A modelling framework for local thermal comfort assessment related to bicycle helmet use. *Journal of Thermal Biology*, 112, 103457 (19 pp.). <https://doi.org/10.1016/j.jtherbio.2022.103457>

This manuscript version is made available under the CC-BY-NC-ND 4.0 license <http://creativecommons.org/licenses/by-nc-nd/4.0/>

A modelling framework for local thermal comfort assessment related to bicycle helmet use

Peter Bröde^a✉, Jean-Marie Aerts^b, Guido De Bruyne^{c,d}, Tiago Sotto Mayor^{e,f}, Simon Annaheim^g, Dusan Fiala^h, Kalev Kuklaneⁱ

^a *Leibniz Research Centre for Working Environment and Human Factors at TU Dortmund (IfADo), Ardeystr. 67, 44139 Dortmund, Germany, ORCID 0000-0001-8107-704X*

^b *Department of Biosystems, KU Leuven, Belgium, ORCID 0000-0001-5548-9163*

^c *Department of Product Development, Faculty of Design Sciences, University of Antwerp, Belgium, ORCID 0000-0002-3594-3258*

^d *Lazer Sport NV, Mechelen, Belgium*

^e *Transport Phenomena Research Centre (CEFT), Engineering Faculty of Porto University, Rua Dr. Roberto Frias, 4200-465 Porto, Portugal, ORCID 0000-0001-8779-1033*

^f *Associate Laboratory in Chemical Engineering (ALiCE), Engineering Faculty of Porto University, Rua Dr. Roberto Frias, 4200-465 Porto, Portugal*

^g *Empa, Swiss Federal Laboratories for Materials Science and Technology, Laboratory for Biomimetic Membranes and Textiles, St. Gallen, Switzerland, ORCID 0000-0002-8192-1391*

^h *Ergosim - Human Thermal Modelling, Messstetten, Germany*

ⁱ *Netherlands Institute for Public Safety (NIPV), Zoetermeer, The Netherlands, ORCID 0000-0003-3169-436X*

✉ Corresponding author: Peter Bröde

Phone +49 231 1084 225; Fax +49 231 1084 400; e-mail: broede@ifado.de; web: <http://www.ifado.de>

Declarations of interest: none

Abbreviations: *clo*: convenient unit for clothing thermal insulation (1 clo = 0.155 m²·K·W⁻¹); *E*: sweat evaporation (W·m⁻²); *E_{max}*: evaporative capacity (W·m⁻²); *GSR*: gross sweat rate (mg·cm⁻²·min⁻¹); *FPC*: Fiala thermal Physiology and Comfort model; *I_{cl}*: intrinsic (or basic) clothing insulation excluding the outer air layer insulation (clo); *I_{t,head}*: headgear total thermal insulation including outer air layer insulation (m²·K·W⁻¹); *I_{a,head}*: air layer thermal insulation of head area (m²·K·W⁻¹); *LSR*: local sweat rate (mg·cm⁻²·min⁻¹); *M*: metabolic rate (W); *n.d.*: non-dimensional; *p_a*: ambient water vapour pressure (Pa); *p_{sk,sat}*: saturated water vapour pressure at skin surface (Pa); *PHS*: Predicted Heat Strain; *PO*: bicycle ergometer power output (W); *R_{et,head}*: headgear total evaporative resistance including air layer (m²·Pa·W⁻¹); *R_{ea,head}*: air layer evaporative resistance of head area (m²·Pa·W⁻¹); *RH*: relative humidity (%); *rmse*: root mean-squared error; *SUD*: sudomotor sensitivity (mg·cm⁻²·min⁻¹·°C⁻¹); Δt_{re} : change in core (rectal) temperature (°C); *t_{sk}*: skin temperature (°C); *t_a*: air temperature (°C); *t_r*: mean radiant temperature (°C); *UTCI*: Universal Thermal Climate Index; *v_a*: air velocity (m·s⁻¹); *w*: skin wettedness (n.d.); *w_{crit,head}*: head skin wettedness comfort threshold (n.d.)

Abstract

Thermal discomfort due to accumulated sweat increasing head skin wettedness may contribute to low wearing rates of bicycle helmets. Using curated data on human head sweating and helmet thermal properties, a modelling framework for the thermal comfort assessment of bicycle helmet use is proposed. Local sweat rates (*LSR*) at the head were predicted as the ratio to the gross sweat rate (*GSR*) of the whole body or by sudomotor sensitivity (*SUD*), the change in *LSR* per change in body core temperature (Δt_{re}). Combining those local models with Δt_{re} and *GSR* output from thermoregulation models, we simulated head sweating depending on the characteristics of the thermal environment, clothing, activity, and exposure duration. Local thermal comfort thresholds for head skin wettedness were derived in relation to thermal properties of bicycle helmets. The modelling framework was supplemented by regression equations predicting the wind-related reductions in thermal insulation and evaporative resistance of the headgear and boundary air layer, respectively. Comparing the predictions of local models coupled with different thermoregulation models to *LSR* measured at the frontal, lateral and medial head under bicycle helmet use revealed a large spread in *LSR* predictions predominantly determined by the local models and the considered head region. *SUD* tended to overestimate frontal *LSR* but performed better for lateral and medial head regions, whereas predictions by *LSR/GSR* ratios were lower and agreed better with measured frontal *LSR*. However, even for the best models root mean squared prediction errors exceeded experimental SD by 18–30%. From the high correlation ($R > 0.9$) of skin wettedness comfort thresholds with local sweating sensitivity reported for different body regions, we derived a threshold value of 0.37 for head skin wettedness. We illustrate the application of the modelling framework using a commuter-cycling scenario, and discuss its potential as well as the needs for further research.

Keywords: thermal comfort, thermoregulation, headgear, sweating, model, local effects

Highlights

- Head sweating is a major concern related to bicycle helmet use and acceptance
- A modelling approach to local thermal comfort assessment is proposed
- Predictions are tested against empirical head sweating data for bicycle helmet use
- Equations are presented to predict wind effects on headgear thermal properties
- Local sweating sensitivity highly correlates with skin wettedness comfort thresholds
- Datasets on head sweating and headgear thermal properties are provided

1 Introduction

1.1 Background

Bicycle helmets effectively reduce the risk of severe head injuries following an accident during cycling (Alfrey et al., 2021; Høye, 2018). However, only 1% to 40% of adult cyclists in European countries make use of bicycle helmets (Bogerd, 2011), where other reports (Otte et al., 2015) suggest a regional pattern with higher usage rates in Nordic compared to South European countries. In Germany, overall helmet use rates increased over the past two decades from less than 5% to more than 30% in 2021 (Evers, 2022) with widely varying rates in different age groups from 76% for 6–10 years old children down to 18% for young adults up to 30 years of age. In addition to other reasons potentially affecting wearing rates like cost, vanity (e.g. hairstyle), simplicity, or general attitudes against helmet use (Ledesma et al., 2019), this may be partly attributable to impaired thermal comfort associated with helmet use (Bogerd et al., 2015a). In addition, in a survey about the attitudes of German cyclists towards bicycle helmet use (Otte et al., 2014), excessive sweating (57%) prevailed over other complaints like impaired visual field (9%) or perceived head pressure (10%). In a recent case series among 72 Canadian unhelmeted injured cyclists (Varriano et al., 2022), 28% of the respondents indicated “discomfort” as a reason for non-wearing a helmet, while 10% stated the helmet would make them sweaty. Therefore, besides epidemiological, psychological and biomechanical aspects of bicycle helmet use (Fahlstedt et al., 2015; Ledesma et al., 2019; Shinar et al., 2018), the EU-funded COST Action TU1101 “Towards safer bicycling through optimization of bicycle helmets and usage” included the investigation of the thermal features of bicycle helmets in a complementary approach consisting of human trials, biophysical testing with thermal manikins or head forms and computer simulation studies (Bogerd et al., 2015b). This work was performed within Working Group 4 ‘Ergonomics of Thermal Effects’ of COST Action TU1101 (Annaheim et al., 2015).

Although increased thermal insulation in the cold (Bogerd et al., 2015a) and attenuated heat gain from sun irradiation (Bogerd et al., 2008; Brühwiler, 2008) were reported as beneficial effects of helmet use on thermal comfort, this contribution will focus on the thermal discomfort in relation to the heat stress associated with cycling in moderate to warm outdoor environments.

Thermal discomfort depends on the skin temperature and thermal sensation in moderate and cold conditions (Gagge et al., 1967, Fanger, 1972), and particularly on sweating and skin wettedness under heat stress, for both the whole body (Gagge et al., 1967; Gagge et al., 1969; Gonzalez and Gagge, 1973; Vargas et al., 2020) and local body regions (Fukazawa and Havenith, 2009; Gerrett et al., 2013). The use of personal protective clothing (Havenith et al., 2008; Holmér, 2006) or local protective equipment (Dotti et al., 2016; Zwolinska, 2013) often hampers the transport of heat and moisture from the skin to the environment, which causes thermal discomfort due to accumulated sweat increasing skin wettedness (Raccuglia et al., 2018b). In this regard, regional differences might occur due to the interplay of local sweating, clothing thermal properties and ventilation (Raccuglia et al., 2018a; Ueda et al., 2006). Skin wettedness (w) is defined as the ratio of the actual heat loss (usually expressed per unit body surface area in terms of $W \cdot m^{-2}$) by sweat evaporation (E) to the evaporation capacity (E_{max}), i.e. the maximum possible evaporative heat loss when the body is entirely covered by sweat. Thus, it can be considered as the fraction of body surface area covered with sweat (Gagge, 1937). Studies relating w to thermal comfort votes indicated that comfort threshold values of skin wettedness (w_{crit}) increased for exercising in comparison to resting conditions, with w_{crit} between 22% and 46% for diverse exercise modes and body regions (Fukazawa and Havenith, 2009; Gerrett et al., 2013; Gonzalez and Gagge, 1973). Because sweat evaporation is closely related to sweat production, local sweat rates should be estimated with high accuracy for a proper assessment of local thermal discomfort in the heat.

Hence, there are a number of topical studies on local sweat production to optimize sportswear, protective clothing or footwear (Machado-Moreira et al., 2008a; Machado-Moreira et al., 2008b; Smith and Havenith, 2011; Smith et al., 2013; Taylor et al., 2006; West et al., 2019). Sweat rates can be modelled depending on (changes in) core and mean skin temperatures and considering the modifying influence of changes in local skin temperature (Nadel et al., 1971). Recent research predicted local sweating based on the so-called sudomotor sensitivity (SUD) (Machado-Moreira et al., 2008b; Taylor et al., 2006; Taylor and Machado-Moreira, 2013), which linearly relates the change in local sweat rate per unit surface area (LSR) to the change in body core temperature (Δt_{re}). A different approach suggests quantifying LSR relative to the gross sweat rate (GSR) of the whole body by providing ratios of LSR/GSR (Smith and Havenith, 2011). However, the latent heat fluxes

related to moisture transport are not integrated into current models of local thermal comfort available for moderate conditions in offices or vehicles (Nilsson, 2007; Zhang et al., 2010a, b), which routinely only consider convective and radiant fluxes, i.e. so-called dry heat losses. Databases of clothing thermal insulation and evaporative resistance usually concentrate on whole-body ensembles (ISO 9920, 2007; Smallcombe et al., 2021), while research on the local thermal properties of clothing is emerging (Fojtlín et al., 2019; Kuklane et al., 2022). In comparison to other body parts, standardized data on headgear thermal properties are almost non-existent e.g., the international standard ISO 9920 (2007) just includes a single entry of thermal insulation for a “cap” without further specification. Furthermore, data on head *LSR* are sparse because the measurement of head sweating by ventilated capsules or moisture absorbent pads (Machado-Moreira et al., 2008b; Morris et al., 2013; Smith and Havenith, 2011) usually require shaving the scalp hair. This might also explain why there are a few studies involving female participants (De Bruyne et al., 2010; De Bruyne et al., 2008). On the other hand, in an emerging ‘virtual ergonomics’ context (Berlin and Kajaks, 2010; Lanzotti et al., 2020; Paul and Wischniewski, 2012), there is an increasing need for numerical approaches involving computer modelling techniques for testing thermal comfort issues as part of the ergonomic assessment of personal protective equipment. This is also stipulated by a recent European standardisation initiative (European Commission, 2012) and a corresponding draft standard (DIN EN 17558:2020-11-Draft, 2020).

1.2 Study objectives

Therefore, the objective of this research was to develop a modelling framework enabling the simulation and assessment of thermal comfort under bicycle helmet use conditions in moderate and warm outdoor environments considering the characteristics of the thermal environment, clothing, level of activity and exposure duration.

Our approach was to review head *LSR* models from the literature and to couple those local models with a whole-body model of thermoregulation predicting Δt_{re} and/or *GSR* (Fiala and Havenith, 2016; Fiala et al., 2012; Fiala et al., 2010; ISO 7933, 2004). Thermal comfort assessment was to be established through the calculation of local skin wettedness (Fukazawa and Havenith, 2009) related to headgear thermal properties (Aljaste et al., 2014; Kuklane et al., 2015), which might depend on relative air velocity (Fonseca, 1974; Havenith and Nilsson, 2004, 2005; Wang et al., 2012). Increased relative air velocities due to cycling

speed are typical under bicycle use conditions, e.g. with the speed of commuting cyclists ranging between 2.8–6.9 m·s⁻¹ (Kuklane et al., 2015). Cycling speed will affect helmet ventilation and is thus highly relevant for the thermal aspects of bicycle helmet use (Brühwiler, 2003; Brühwiler et al., 2006; Martínez et al., 2016).

The modelling work was supplemented by testing the predictions of local sweat rates against published data, by the derivation of comfort criteria for the head region in contact with the helmet, by constructing a catalogue of data curated within the COST Action TU1101 network concerning the wind effects on headgear thermal properties, and by a use case implementation of a commuter-cycling scenario as an example application.

2 Material and Methods

2.1 Head sweat rate prediction models

As head sweat rates are usually measured at the shaved scalp, data and models on head sweating are sparse for males and absent for females. Following a literature review (Bogerd et al., 2015a), six different models based on sudomotor sensitivities (*SUD*) applicable to the frontal, lateral and medial head regions were determined (Machado-Moreira et al., 2008b; Smith and Havenith, 2011; Taylor and Machado-Moreira, 2013), which were developed based on data from different cycling or treadmill exercising protocols or resting conditions. An additional set of three models expressed *LSR* as ratios to the gross sweat rate (*GSR*) of the whole body. One model estimated *LSR* as equal to *GSR*, i.e. *LSR/GSR*=1 (Taylor and Machado-Moreira, 2011), while two additional *LSR/GSR* ratios were derived from a study with exercising participants (Smith and Havenith, 2011). Table 1 lists the local models and their sources.

Table 1. Sources with references to the literature and descriptions of models predicting local sweat rates (*LSR*) at the head via sudomotor sensitivities (*SUD*) and as the ratio of *LSR* to gross sweat rate (*GSR*), respectively.

Identifier	Source	Description of conditions
SUD1	Ref1	45 min incremental cycling protocol (50-100 W) in the heat (n=10)
SUD2	Ref2	30 min treadmill running at 55% VO _{2max} @25°C, n=9 (frontal), n=4 (lateral, medial head)
SUD3	Ref2	30 min running at 75% VO _{2max} subsequent to SUD2
SUD4	Ref2	Overall results from combined SUD2 & SUD3 protocol
SUD5	Ref3	Cycling in the heat at 125 W (n=46)
SUD6	Ref3	Resting in the heat (n=49)
GSR1	Ref3	<i>LSR</i> set equal to <i>GSR</i>
GSR2	Ref2	Conditions identical to SUD2

Notes: Ref1: Machado-Moreira et al. (2008b); Ref2: Smith and Havenith (2011); Ref3: Taylor and Machado-Moreira (2013); n: sample size in experiments underlying the parameter; VO_{2max} : maximum oxygen uptake

2.2 Head thermal comfort modelling

To predict head *LSR* depending on the parameters of the thermal environment, clothing, activity and exposure duration, the local models in Table 1 require the input of core temperature change (Δt_{re}) and gross sweat rate (*GSR*), respectively.

By connecting the head *LSR* prediction with the calculation of local skin wettedness concerning the helmet's thermal properties, we propose a modelling framework for the assessment of head thermal comfort consisting of five steps. The flowchart in Figure 1 presents the elements of this stepwise approach with the input and output variables, and the links to the governing equations, tables and sections of this paper. In addition, it includes the supplemental validation of head perspiration prediction, the meta-analysis on wind effect on headgear thermal properties, and the derivation of a skin wettedness comfort threshold for the head region, respectively, as described in the following sections.

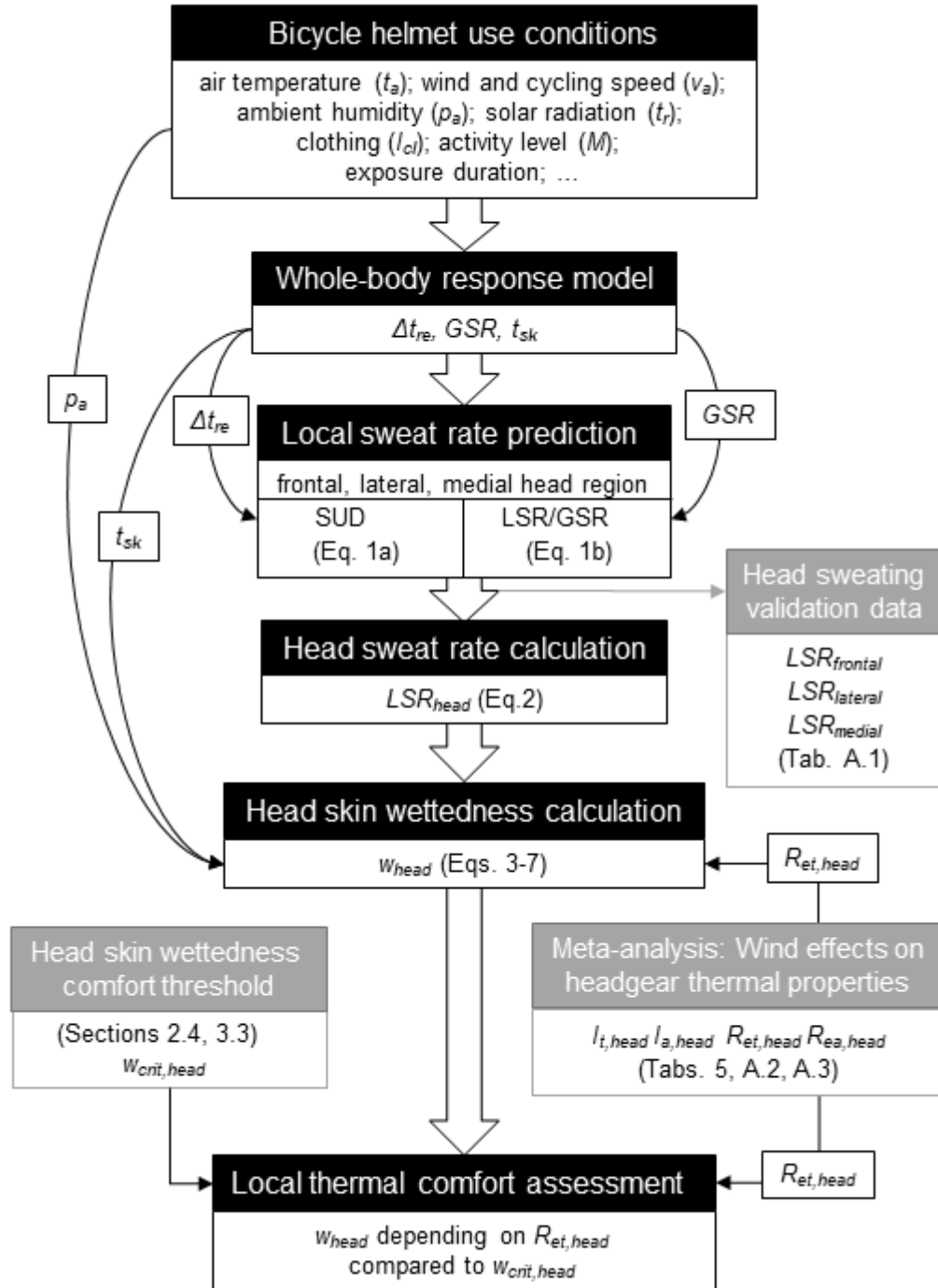


Figure 1. Elements of the proposed modelling framework for local thermal comfort assessment under bicycle helmet use conditions. From top to bottom, the flowchart depicts the modelling steps with references to input and output variables (cf. list of abbreviations) and governing equations, tables and supplemental information. Grey shaded boxes indicate the supplemental analyses concerning the validation data on head perspiration, the meta-analysis on wind effect on headgear thermal properties, and the derivation of a skin wettedness comfort threshold for the head region, respectively.

2.2.1 Step 1: Simulation of whole-body responses

The initial step comprises the simulation of whole-body responses (Δt_{re} , GSR) depending on the parameters of the thermal environment, clothing characteristics, activity level, and

exposure duration. In this paper, we will apply different models with varying complexity as recently reviewed (Havenith and Fiala, 2016) and described below in section 2.3.

2.2.2 Step 2: LSR predictions

From Δt_{re} and GSR , we predict frontal, lateral, and medial head LSR (in $\text{mg}\cdot\text{cm}^{-2}\cdot\text{min}^{-1}$) using a local model from Table 2 by multiplying the corresponding sudomotor sensitivity (SUD) coefficients with Δt_{re} or the LSR/GSR ratio with GSR , respectively, according to the following equations:

$$LSR_{region} = SUD_{region} \times \Delta t_{re} \quad \text{in } \text{mg}\cdot\text{cm}^{-2}\cdot\text{min}^{-1} \quad \text{Eq. 1a}$$

$$LSR_{region} = (LSR/GSR)_{region} \times GSR \quad \text{in } \text{mg}\cdot\text{cm}^{-2}\cdot\text{min}^{-1} \quad \text{Eq. 2b}$$

In Eqs. 1a & 1b, the subscript *region* denotes the coefficients and resulting local sweat rates corresponding to the frontal, lateral, and medial head region, respectively.

Table 2. Coefficients for predicting local sweat rates (LSR) at the frontal, lateral and medial head regions via sudomotor sensitivities (SUD) and as the ratio of LSR to gross sweat rate (GSR), respectively (n.d.: non-dimensional).

Identifier	Head region		
	frontal	lateral	medial
Sudomotor sensitivity ($\text{mg}\cdot\text{cm}^{-2}\cdot\text{min}^{-1}\cdot^{\circ}\text{C}^{-1}$)			
SUD1	1.89	1.93	1.06
SUD2	1.96	0.90	0.48
SUD3	5.31	2.31	1.92
SUD4	3.76	1.47	1.01
SUD5	1.55	1.03	0.55
SUD6	1.65	0.52	0.27
LSR / GSR ratio (n.d.)			
GSR1	1	1	1
GSR2	2.61	1.20	0.64
GSR3	2.60	1.16	0.81

2.2.3 Step 3: Computation of head LSR

LSR for the head region in contact with the helmet is computed as area-weighted mean applying a 1:2:4 weighing for frontal, lateral and medial LSR as deduced from research with head manikins (Martínez et al., 2016) and shown in Eq. 2:

$$LSR_{head} = (1 \times LSR_{frontal} + 2 \times LSR_{lateral} + 4 \times LSR_{medial}) / 7 \quad \text{in } \text{mg}\cdot\text{cm}^{-2}\cdot\text{min}^{-1} \quad \text{Eq. 2}$$

2.2.4 Step 4: Calculation of head skin wettedness

Considering the offset in skin wettedness of 6% caused by diffusive moisture transport (Parsons, 2014), we calculate head skin wettedness (w_{head}) according to Eq. 3:

$$w_{head} = 0.06 + 0.94 \times (E_{head} / E_{max}) \quad \text{Eq. 3}$$

In Eq. 3, E_{head} denotes the head evaporative heat loss, computed by Eq. 4 with $\lambda = 2430$ J/g, representing the latent heat per gram of evaporated sweat and (1/6) converting the LSR unit from $\text{mg}\cdot\text{cm}^{-2}\cdot\text{min}^{-1}$ to $\text{g}\cdot\text{s}^{-1}\cdot\text{m}^{-2}$, as shown below:

$$E_{head} = \lambda \times LSR_{head} \times (1/6) \quad \text{in } \text{W}\cdot\text{m}^{-2} \quad \text{Eq. 4}$$

E_{max} in Eq. 3 is the maximum possible evaporative heat loss, depending on the water vapour pressure gradient between the skin, which is assumed to be saturated with sweat, and the environment, and on $R_{et,head}$ ($\text{m}^2\cdot\text{Pa}\cdot\text{W}^{-1}$) representing the evaporative resistance of the head area covered by the helmet plus the resistance of the surface air layer (ISO 9920, 2007).

$R_{et,head}$ will require corrections for the wind effects inherent to bicycle helmet use conditions due to cycling speed. Though these corrected values are sometimes termed ‘resultant’ evaporative resistance (ISO 9920, 2007), in this paper we adhere to the abbreviation $R_{et,head}$. We developed corresponding predictive equations with the methodology as outlined in section 2.5 and the resulting regression functions presented by Table 5 in section 3.4. E_{max} can then be calculated as:

$$E_{max} = (p_{sk,sat} - p_a) / R_{et,head} \quad \text{in } \text{W}\cdot\text{m}^{-2} \quad \text{Eq. 5}$$

In Eq. 5, p_a and $p_{sk,sat}$ denote the ambient and saturated skin water vapour pressure (in Pa), respectively, which were calculated from relative humidity (RH), air temperature (t_a) and skin temperature (t_{sk}) applying the Antoine-equation using the formula presented in Havenith (2004) as shown in Eqs. 6 & 7:

$$p_{sk,sat} = \exp(23.5613 - \frac{4030183}{t_{sk}+235}) \quad \text{in Pa} \quad \text{Eq. 6}$$

$$p_a = \exp(23.5613 - \frac{4030183}{t_a+235}) \times RH/100 \quad \text{in Pa} \quad \text{Eq. 7}$$

2.2.5 Step 5: Thermal comfort assessment

Finally, we perform the thermal comfort assessment by relating w_{head} to $R_{et,head}$ and comparing it to the comfort threshold $w_{crit,head}$ of head skin wettedness. Here, it is essential

to consider the effect of relative air movements due to cycling speed, which will reduce $R_{et,head}$ as outlined in section 2.5 below. Details for the derivation of $w_{crit,head}$ are provided in section 2.4.

2.3 Validation of LSR predictions against observed data

To check the validity of the predicted LSR, i.e. the first two steps of the modelling framework presented in the previous section (2.2.1 and 2.2.2), we compared the predictions of the resulting models with individual LSR measurements from exercising subjects under realistic conditions, i.e. while wearing a bicycle helmet on an unshaved scalp. These data were collected during a laboratory study described in detail elsewhere (De Bruyne et al., 2008) so we will only briefly repeat the relevant information here.

Five males and four females with a mean (SD) age of 26.7 (3.5) years completed in triplicate an identical protocol consisting of two consecutive bouts of 20 minutes exercise on a bicycle ergometer. The first bout was performed under a *low* workload with a power output (PO) of 80 W for females and 100 W for males, subsequently followed by a second bout of *high* workload with PO of 120 W (females) and 150 W (males), respectively. Thermal conditions were set to air temperature (t_a) of 20 °C, relative humidity (RH) of 40%, air velocity (v_a) of 3 m·s⁻¹, and mean radiant temperature was equal to air temperature. The characteristics of the climatic chamber had been described before (De Bruyne et al., 2008, 2010), with control accuracy indicated by the SD reported as 0.1 °C (t_a), 0.6% (RH), 0.2 m·s⁻¹ (v_a), respectively.

In addition to the helmet, the participants wore T-shirt, shorts, underwear, socks, and sport shoes with the ensemble's basic (or intrinsic) thermal insulation estimated as $I_{cl} = 0.4$ clo (1 clo = 0.155 m²·K·W⁻¹) using standard tables (ISO 9920, 2007). Because all the whole-body models require the input of metabolic rate (M), the latter was calculated from power output (PO), assuming a typical gross cycling efficiency ($=PO/M$) of 20% (Ettema and Loras, 2009).

Local sweat rates at the frontal (forehead), lateral (temple) and medial (occipital and parieto-occipital) head regions were measured continuously with ventilated capsules connected to a sweat rate monitor (Model SKD-4000; Skinco Co Ltd, Nagoya, Japan). The recordings averaged over the final three minutes of each exercise bout were stored for later analyses. Each participant performed the experiment in triplicate. However, due to several missing values, less than the maximum possible 27 measurements per workload condition

and head region were available, as shown in Table 3. As the medial head region comprised two measurement sites, the difference of available (n) to the maximum possible number of measurements (54) is even higher, indicating difficulties in obtaining reliable local sweat rate recordings from a scalp covered by hair underneath a bicycle helmet. The overall 130 individual *LSR* observations are listed in the appendix as Table A.1 and summarized concerning head region and workload by Table 3.

Table 3. Summary statistics for the data from Table A.1 with the number of measurements (n), means, standard deviations (SD), minimum (Min) and maximum (Max) values of local sweat rates observed (*LSR_{obs}*) at the frontal (forehead), lateral (temple) and medial head regions under low and high workload conditions (De Bruyne et al., 2008).

Workload	Head region	n	<i>LSR_{obs}</i> ($mg \cdot cm^{-2} \cdot min^{-1}$)			
			Mean	SD	Min	Max
low	frontal	22	0.56	0.40	0.06	1.80
	lateral	23	0.56	0.53	0.03	2.21
	medial	20	0.78	0.64	-0.06	2.37
high	frontal	21	1.18	0.68	0.33	2.73
	lateral	23	1.20	0.90	0.30	3.41
	medial	21	1.72	0.93	0.04	3.51

For considering the influence of the whole-body model, we calculated the whole-body responses (Δt_{re} , *GSR*) required as input for local sweat rate prediction according to Table 2 using three different models, (i) the “Predicted Heat Strain” (PHS) from ISO 7933 (2004), a heat index based on the analysis of human heat balance considering clothing thermal properties and their modifications by wind and body movements (D'Ambrosio Alfano et al., 2016), and also including a prediction of Δt_{re} and *GSR*, ‘which puts it closer to a physiological model’ (Havenith and Fiala, 2016); (ii) the multi-node UTCI-Fiala model of thermoregulation (Fiala et al., 2012), which had been extensively validated (Kampmann et al., 2012; Psikuta et al., 2012) while developing the Universal Thermal Climate Index UTCI (Bröde et al., 2012); and (iii) the still more elaborated “Fiala thermal Physiology and Comfort” (FPC) model (Fiala and Havenith, 2016; Fiala et al., 2010).

Predictions of Δt_{re} and *GSR* were calculated by PHS using the BASIC program as printed in the standard (ISO 7933, 2004; Malchaire and Piette, 2004), while for UTCI-Fiala and FPC, Dusan Fiala provided the software based on the published models (Fiala and Havenith, 2016; Fiala et al., 2012; Fiala et al., 2010). The environmental and time dependent workload parameters as well as clothing properties were set according to the conditions of the experiments.

Corresponding to the measurement protocol (De Bruyne et al., 2008), the predictions of both Δt_{re} and GSR were averaged over the final 3 minutes of each exposure period. They were then linked with the nine different local models (Table 2) to compute the predictions LSR_{pred} . Thus, we obtained 27 predictions (9 local models \times 3 whole-body models) for each observed frontal, lateral and medial LSR_{obs} .

The prediction error was then computed as $LSR_{pred} - LSR_{obs}$ with positive values indicating overestimation and negative values indicating underestimation, respectively. Prediction errors were summarized as mean (*bias*) and root-mean-squared errors (*rmse*). These were compared to pooled experimental standard deviation (SD_{pooled}), which was calculated from the information in Table 3 according to Eq. 8, where (SD_{low} , SD_{high}) and (n_{low} , n_{high}) denote standard deviations and number of observations recorded for low and high workloads, respectively.

$$SD_{pooled} = \sqrt{\frac{(n_{low}-1) \times SD_{low}^2 + (n_{high}-1) \times SD_{high}^2}{n_{low} + n_{high} - 2}} \quad \text{Eq. 8}$$

In addition, we derived corresponding measures for prediction bias and rmse for the covered head region as area-weighted values applying the 1:2:4 weighting to the individual prediction errors for the frontal, lateral and medial region, respectively, as applied before in Eq. 2 of section 2.2.3.

To assess the prediction error subject to the head regions, the local and whole body models, the intra- and inter-individual variability as well as the residual variance, we performed a variance component analysis of the prediction error using linear mixed models (Littell et al., 2006).

2.4 Head skin wettedness comfort threshold

Data on human head perspiration are scarce as indicated by the small sample sizes underlying the local models (Table 1). Therefore, head skin wettedness comfort threshold values ($w_{crit,head}$) are not readily available, so they have to be estimated. We studied the relationship of local comfort threshold values for skin wettedness (w_{crit}) with local sweating sensitivity performing linear regression analyses. This approach linked experimentally derived whole-body w_{crit} and local w_{crit} for the arms, legs, frontal and back trunk (Fukazawa

and Havenith, 2009) to their corresponding log-transformed LSR/GSR ratios. In accordance with GSR2 from Table 2, we used the LSR/GSR values for the whole body, as well as for arms, legs, frontal and back trunk from the original study (Smith and Havenith, 2011). The LSR/GSR ratio for the covered head region was computed as the area-weighted average of the frontal, lateral and medial head values (Table 2) using weights as in Eq. 2, yielding a value of 1.08. We put this value into the regression equation to calculate the threshold value for the head ($w_{crit,head}$).

2.5 Meta-analysis of wind effects on headgear thermal properties

By searching the literature and the archives of COST Action TU1101 members, we compiled a database presented in the appendix as Table A.2 on head total thermal insulation ($I_{t,head}$) and evaporative resistance ($R_{et,head}$) measured under varying air velocities (v_a). All measurements were performed using thermal manikins or head forms with different bicycle helmets (Aljaste et al., 2015; Kuklane et al., 2015; Liu and Holmér, 1997; Martinez, 2016; Mukunthan et al., 2019). To enlarge the database, we considered other types of headgear as well, including helmets worn in military (Chen et al., 2006; Fonseca, 1974; Zwolinska et al., 2014), industrial (Liu and Holmér, 1995, 1997; Ueno and Sawada, 2019) and sports activities (Pang et al., 2014).

We complemented these data with values of head-level boundary air layer thermal insulation ($I_{a,head}$) and evaporative resistance ($R_{ea,head}$) as shown in Table A.3. These data were obtained from reports on measurements with nude manikins or head forms (Aljaste et al., 2015; Brühwiler, 2003; Fonseca, 1974; Kuklane et al., 2015; Liu and Holmér, 1995; Lu et al., 2015; Martinez, 2016; Mukunthan et al., 2019; Pang et al., 2014; Psikuta et al., 2016; Ueno and Sawada, 2019; Wang et al., 2012; Zwolinska et al., 2014).

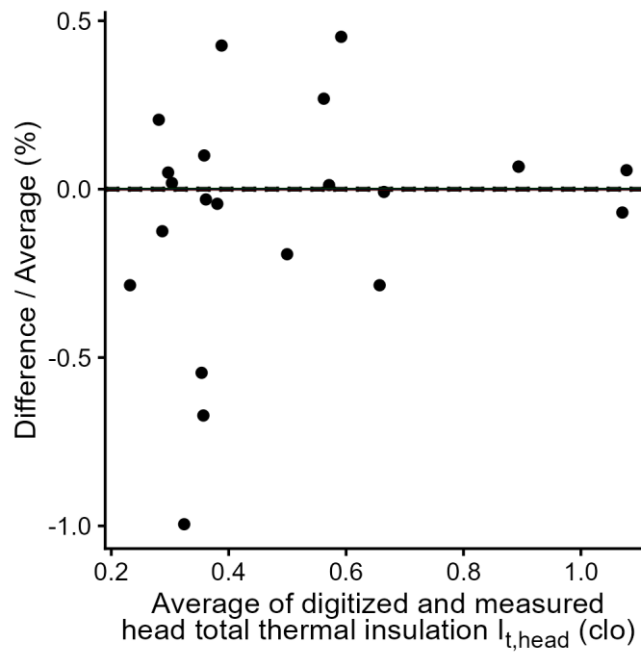


Figure 2. Percentage deviations between digitized and measured values of head total thermal insulation ($I_{t,head}$) in clo units ($1 \text{ clo} = 0.155 \text{ m}^2 \cdot \text{K} \cdot \text{W}^{-1}$) from the measurements reported by Kuklane et al. (2015), cf. Tables A.2 & A.3, with the dashed horizontal line indicating median bias.

We compiled the database by transcribing values published as tables and digitizing values published as figures using Digitizelt (Borman, 2016). Although this software has been previously shown to deliver reliable results (Rakap et al., 2016), we compared total head thermal insulation measurements performed within COST Action TU1101 and reported by Kuklane et al. (2015) to the corresponding digitized values from Tables A.2 & A.3. Figure 2 reveals a negligible median bias with absolute percentage deviations below 1% for all measurements, thus pointing to the validity of our data gathering approach.

We derived log-log-linear regression equations predicting the local thermal properties by air velocity considering the within-study correlation by random coefficient mixed models (Littell et al., 2006).

2.6 Application to commuter cycling as a use case

As use case, we exemplify the application of our approach by considering the results of a study looking at the energy expenditure during commuter cycling (de Geus et al., 2007). We simulated a person cycling for 30 minutes with 125 W power output assuming 20% cycling gross efficiency (Ettema and Loras, 2009) as in section 2.3. The climatic conditions considered for the simulation were an air temperature of 20 °C, a relative humidity of 40%,

corresponding to water vapour pressure of 936 Pa, shaded condition (mean radiant temperature = air temperature), and (relative) air velocity of $v_a = 6 \text{ m}\cdot\text{s}^{-1}$ corresponding to a cycling speed of 21.6 km/h in still air. The latter was within the range of 2.8–6.9 $\text{m}\cdot\text{s}^{-1}$ reported as representative during commuter cycling (Kuklane et al., 2015; de Geus et al., 2007). Basic clothing insulation was set to $I_{cl} = 0.4 \text{ clo}$ in accordance with the experimental settings from section 2.3 (De Bruyne et al., 2008). For studying the influence of convective effects, comparative simulations were carried out for $v_a = 0.3 \text{ m}\cdot\text{s}^{-1}$ as low air velocity condition typically applied for standardized measurements of headgear thermal properties (Chen et al., 2006; Fonseca, 1974; Kuklane et al., 2015; Pang et al., 2014). Note that this would represent a realistic setting only in the hypothetical case with wind from the back almost exactly compensating for the relative air movement due to cycling speed.

We performed the modelling steps 1–5 from section 2.2 using the UTCI-Fiala model (Fiala et al., 2012) for the simulation of whole-body responses (Δt_{re} , GSR , mean t_{sk}). This model was coupled with the local models from Table 2 by using the simulated mean t_{sk} as a proxy for head t_{sk} as input to Eq. 6 when computing head skin wettedness (Figure 1).

3 Results

3.1 Local sweat rate models

Comparing the coefficients of the nine local models (Table 2) for the different head regions showed considerable variability between the models. However, a general pattern emerged with higher sweating sensitivity at the forehead compared to the lateral head, and lower values for the medial area inside the hairline. This was in contrast to the summarized experimental data from Table 3, indicating the highest sweat rates recorded at the covered medial head. The sweat rates at the frontal and lateral head regions, which were less covered by hair and helmet and thus more prone to convective cooling, were reduced to very similar values in the experiments. This qualitative comparison points towards an imbalance between the local models and the summarized measurements concerning the regional sweat distribution at the head. The potential consequences of this observation are quantified in the next section.

3.2 Validation of LSR predictions

3.2.1 Whole body model output

Table 4 presents the predictions of the change in core temperature from resting baseline (Δt_{re}) and gross sweat rates (GSR) related to the workload conditions and whole-body models. As expected, all models predicted higher strain for the high workload condition at the end of the second bout. Similarly, though to a minor degree, higher strain was predicted for the higher power output settings applied to males in comparison to female participants, with very low to nil sweating for the 80 W condition. Inter-model differences were smaller compared to the influence of workload, with PHS predicting slightly higher core temperatures and lower sweat rates compared to the advanced models, especially under high workload.

To consider the potential effect of an increased clothing insulation caused by wearing a helmet, we also simulated these conditions using PHS with $I_{cl} = 0.6$ clo. However, we observed only minor changes in GSR , which increased by 0.02 to 0.06 $\text{mg}\cdot\text{cm}^{-2}\cdot\text{min}^{-1}$, and in Δt_{re} , which concomitantly decreased by 0.01 to 0.06 $^{\circ}\text{C}$. So, we continued with our subsequent analyses using $I_{cl} = 0.4$ clo.

Table 4. Core temperature increase (Δt_{re}) and gross sweat rate (GSR) predicted by the whole-body models PHS, UTCI-Fiala and FPC, respectively, at the end of the cycling periods for the gender-specific workload conditions with specified power output (De Bruyne et al., 2008) assuming 20% gross cycling efficiency. Note that FPC predicted zero sweating for the 80 W (low-female) power output setting.

Workload	Gender / Power output	Δt_{re} ($^{\circ}\text{C}$)			GSR ($\text{mg}\cdot\text{cm}^{-2}\cdot\text{min}^{-1}$)		
		PHS	UTCI	FPC	PHS	UTCI	FPC
low	female / 80 W	0.57	0.46	0.29	0.038	0.061	0.000
	male / 100 W	0.66	0.58	0.43	0.064	0.128	0.035
high	female / 120 W	0.92	0.81	0.84	0.156	0.234	0.214
	male / 150 W	1.20	1.05	1.16	0.266	0.379	0.343

3.2.2 LSR prediction error analysis

Figure 3a illustrates the twenty-seven (3 whole-body models \times 9 local models) LSR predictions for each observation at the frontal, lateral, and medial head regions compared to the empirical values from Table A.1. We observed a considerable variability between the tested models, with a ten-fold increase from the lowest to the highest predicted LSR in all conditions. Comparison to the identity line indicated a tendency for overestimation for the

frontal, underestimation for the medial and a more balanced outcome for the lateral head region. The results of the variance component analysis on the factors influencing the LSR prediction error (Figure 3b) indicate that about two-thirds of the error variance could be attributed to the effect of the head region, the local model and their interaction. The remaining components are dominated by inter- and intra-individual as well as residual variability, whereas the influence of the different whole body models and the workload nested within gender on LSR prediction error appeared negligible.

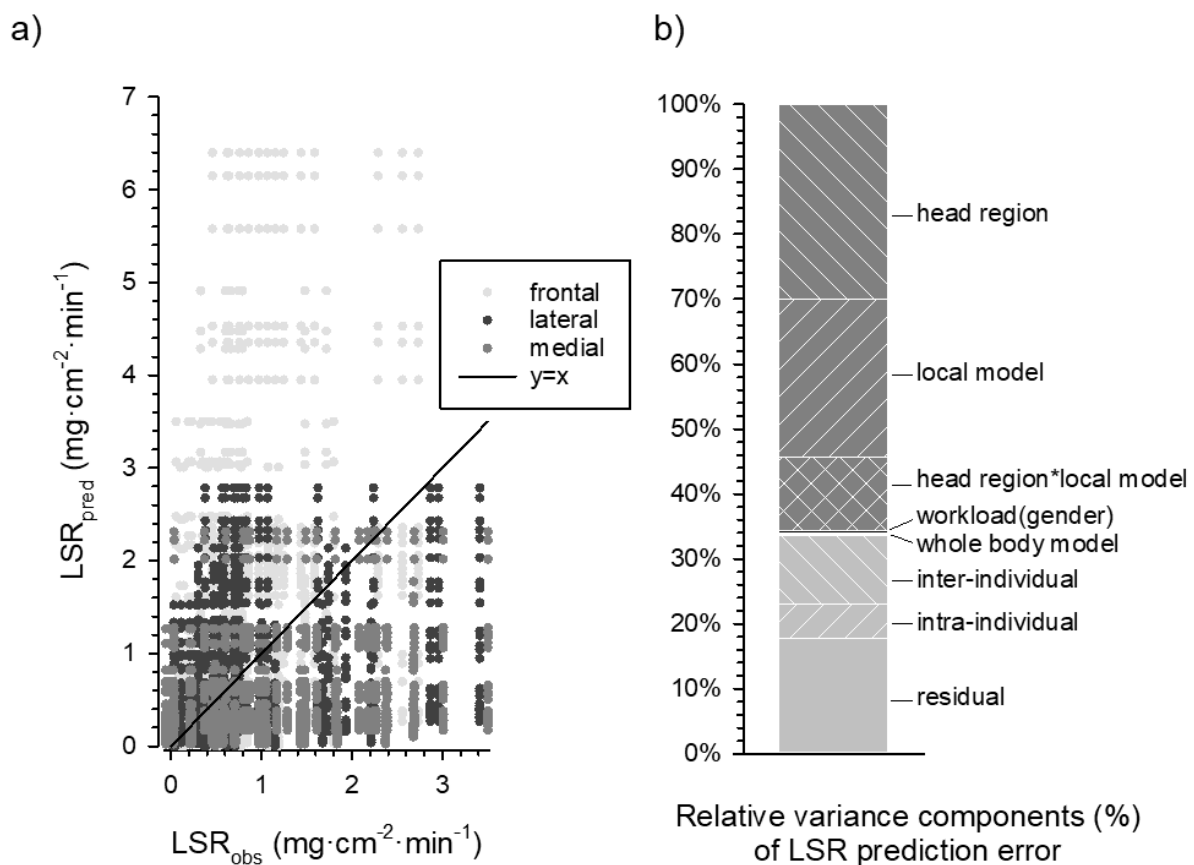


Figure 3. (a) Twenty-seven (3 whole-body models \times 9 local models) predictions of local sweat rates (LSR_{pred}) for each condition at the frontal, lateral and medial head regions compared to the corresponding observed values (LSR_{obs}) from Table A.1. (b) Results of the variance component analysis with a decomposition of the LSR prediction error ($=LSR_{pred} - LSR_{obs}$) indicating the relative influence of the head region, the local models and their interaction, as well as of the workload conditions and whole-body models compared to the inter-individual, intra-individual and residual variance (the latter including all other two-way and higher-order interaction terms).

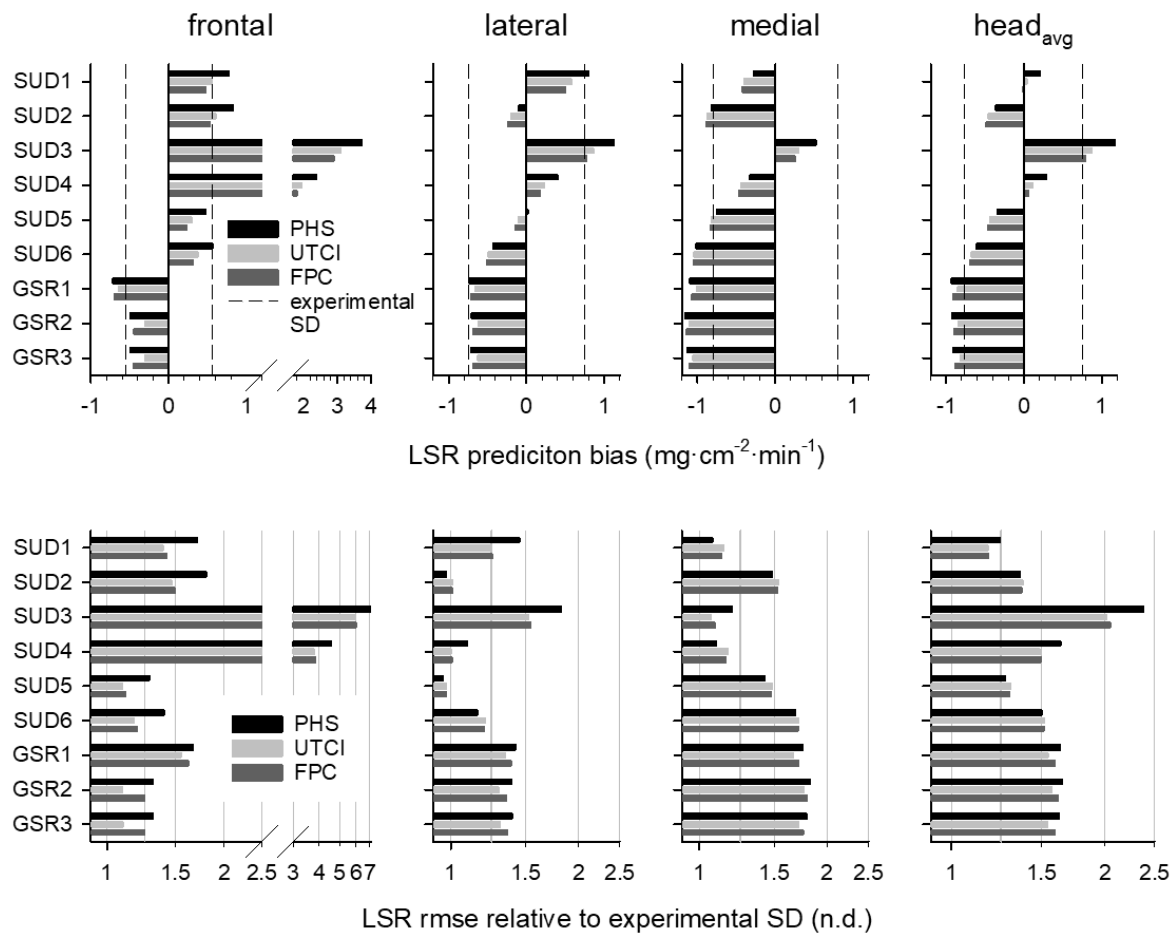


Figure 4. Mean *LSR* prediction error (bias, upper panel) with positive values indicating overestimation and negative values indicating underestimation of measured *LSR* compared to the experimental SD (vertical reference lines), and root-mean-squared error (rmse, lower panel). Data were pooled for the low and high workload conditions (Eq. 8). Calculations were performed with nine local models (Table 2) coupled with the whole-body models PHS, UTCI-Fiala and FPC, respectively, for the frontal, lateral and medial regions. Statistics for the covered head area (*head_{avg}*) were computed from the regional prediction errors as area-weighted average using the weighing scheme from Eq. 2.

Figure 4 displays the predictive accuracy in terms of bias and rmse relative to experimental SD in relation to the local and whole-body models for the frontal, lateral, medial and area-weighted averaged covered head regions, respectively. As the influence of gender and workload had turned out to be negligible in the variance component analysis (Figure 3b), we present the results pooled over the workload conditions.

All six models based on sudomotor sensitivity overestimated frontal head *LSR*, whereas a more balanced pattern emerged for the lateral region. On the other hand, medial *LSR* was underestimated by all but one (SUD3) model, with SUD1 and SUD5 showing absolute bias below empirical SD at all head regions, at least in connection with the advanced whole-body models. These two local models also exhibited reasonable accuracy in terms of bias for the

covered head ($head_{avg}$), as it also occurred for SUD2 and SUD4. Still, the latter showed more significant bias in the medial and frontal regions, respectively.

GSR-based models predicted lower LSR compared to SUD yielding higher accuracy with slight underestimation at the forehead, where regionally varying sensitivity coefficients (GSR2, GSR3) outperformed the simple setting $LSR = GSR$ (GSR1). However, the underestimation error increased at the lateral and medial regions exceeding experimental SD at the latter and for the area-weighted overall value ($head_{avg}$), which is determined to a great extent by the medial error values (cf. Eq. 2).

Consequently, overall head rmse for GSR models exceeded empirical SD by about 50%, resembling the accuracy of some SUD models (SUD4, SUD6), while SUD1 exhibited the lowest overall rmse of 18% above empirical SD, followed by SUD5 with about 30%.

As expected from the variance component analysis (Figure 3b), variability among the whole-body models was marginal, with a tendency of prediction bias involving PHS more often outside experimental SD than for the advanced models. A slightly superior performance was observed for the UTCI-Fiala model in connection with GSR local models.

3.3 Head skin wettedness comfort threshold

Figure 5 shows that skin wettedness comfort thresholds w_{crit} reported by Fukazawa and Havenith (2009) for the whole body, frontal and back torso, arms and thighs were highly positively correlated ($R>0.9$) with sweating sensitivity expressed as LSR/GSR ratio GSR2 (Smith and Havenith, 2011). As outlined in section 2.4, the corresponding ratio for the covered head region amounted to 1.08. Using this value as input to the derived regression equation yielded $w_{crit,head} = 0.37$ as comfort threshold for head skin wettedness. Notably, applying the GSR3 sensitivities from Tables 1&2 or using averaged GSR2 and GSR3 values in this analysis yielded similar values for $w_{crit,head}$ between 0.37-0.38, suggesting that threshold values were robust in the context of the chosen local model.

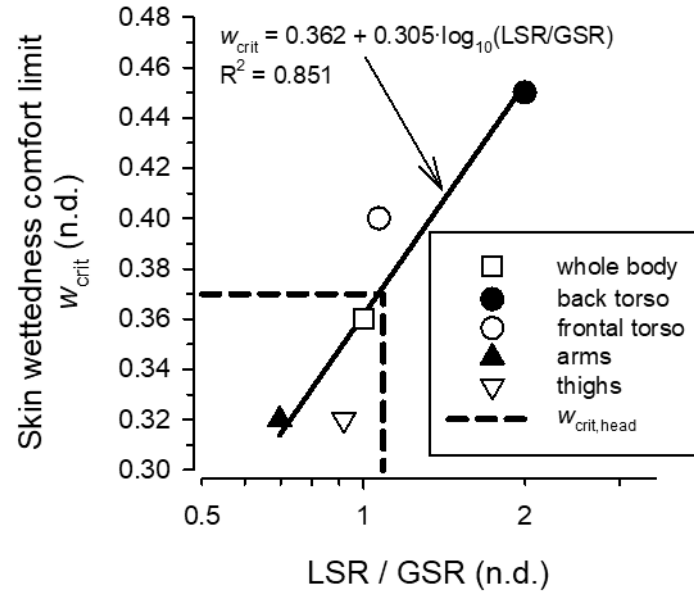


Figure 5. Regression of skin wettedness comfort limits (w_{crit}) for various body parts (Fukazawa and Havenith, 2009) on sweating sensitivity (GSR2 from Table 1) with derived $w_{crit,head}$.

3.4 Wind effects on headgear thermal properties

Figure 6 presents the headgear total thermal insulation and evaporative resistance values from different sources as listed in Table A.2 depending on air velocity. Figure 7 shows the corresponding values reported for the nude head from Table A.3 representing air layer thermal insulation and evaporative resistance, respectively.

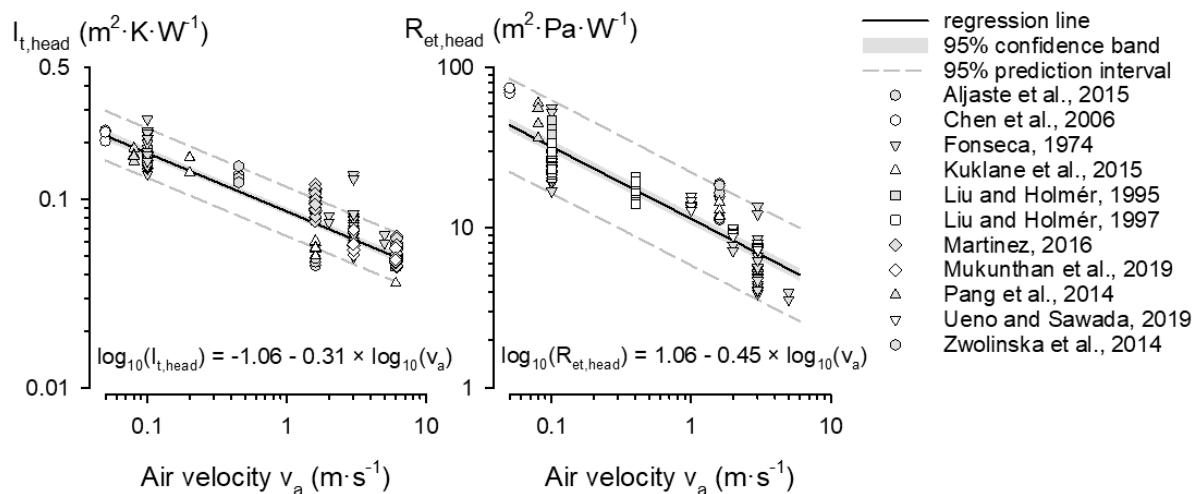


Figure 6. Meta-analysis of the effect of air velocity (v_a) on headgear's total thermal insulation ($I_{t,head}$, left panel), and evaporative resistance ($R_{et,head}$, right panel) presenting log-log-linear regression equations with 95% confidence bands for the regression lines as derived from published measurements with varying headgear using random coefficient mixed models.

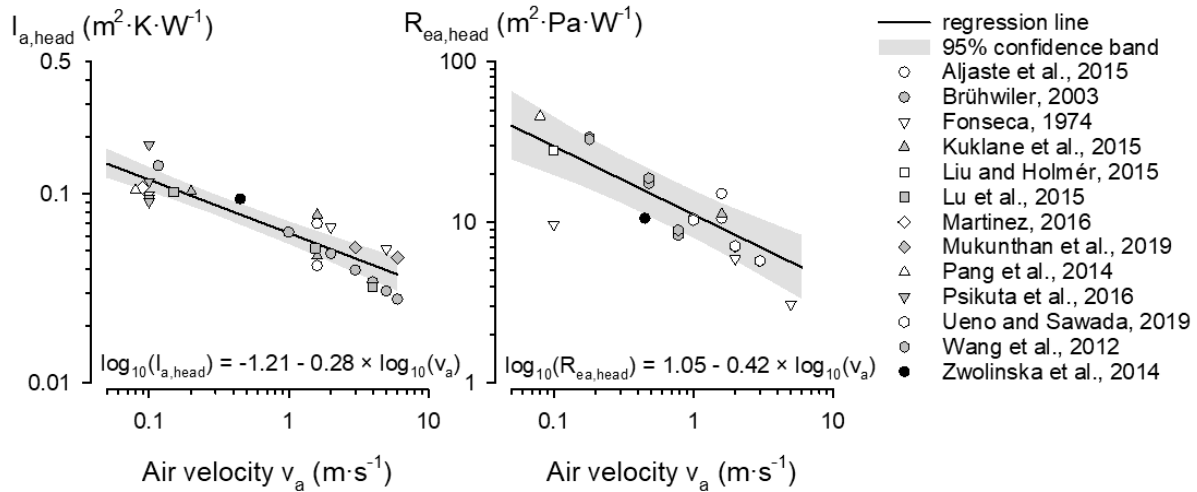


Figure 7. Meta-analysis of the effect of air velocity (v_a) on boundary air layer thermal insulation ($I_{a,head}$, left panel), and evaporative resistance ($R_{ea,head}$, right panel) at uncovered head level. Log-log-linear regression equations with 95% confidence bands for the regression lines were derived from published measurements with nude manikins or head forms using random coefficient mixed models.

As expected, increasing air velocity (v_a) decreased thermal insulation and evaporative resistance, and the narrow 95% confidence bands indicate that this relation was reasonably fitted by log-log-linear regression lines with intercept α and slope β as shown in Table 5. The wider 95% prediction intervals relevant for predictions for a particular item of headgear were omitted from Figure 7 for legibility purposes. Note that values for still air conditions ($v_a = 0.1 \text{ m}\cdot\text{s}^{-1}$) can be computed as $10^{(\alpha-\beta)}$. Air velocities listed in Tables A.2 & A.3 varied between $0.05\text{--}6.1 \text{ m}\cdot\text{s}^{-1}$, thus marking the range of valid applications for the derived equations, closely fitting to the speed representative for commuter cycling (Kuklane et al., 2015).

Interestingly, the slightly more negative slopes (β) obtained for headgear coincide with recently reported (Kuklane et al., 2015) lower thermal insulation values for optimized bicycle helmets under elevated wind speed compared to measurements with a nude head form.

Table 5. Regression results for the effects of air velocity (v_a) on headgear thermal insulation ($I_{t,head}$) and evaporative resistance ($R_{et,head}$) as well as on head boundary air layer thermal insulation ($I_{a,head}$) and evaporative resistance ($R_{ea,head}$). Estimates of intercept (α) and slope (β) with standard errors (SE) and P-values were obtained by fitting log-log-linear regression functions $\log_{10} y = \alpha + \beta \times \log_{10} v_a$ to the data from Table A.2 and Table A.3.

y	α (SE)	$P_{ \alpha =0}$	β (SE)	$P_{ \beta =0}$
$I_{t,head}$	-1.06 (0.01)	<.0001	-0.31 (0.01)	<.0001
$R_{et,head}$	1.06 (0.02)	<.0001	-0.45 (0.01)	<.0001
$I_{a,head}$	-1.21 (0.03)	<.0001	-0.28 (0.03)	<.0001

y	α (SE)	$P_{ \alpha=0}$	β (SE)	$P_{ \beta=0}$
$R_{ea,head}$	1.05 (0.06)	<.0001	-0.42 (0.07)	<.0001

3.5 Use case – thermal comfort assessment for commuter cycling

Predicted core temperature responses were almost identical with $\Delta t_{re} = 0.9$ °C at the end of the simulated 30 min exposure for the different air velocities. On the other hand, gross sweat rate was reduced at higher wind speed from 0.38 to 0.27 mg·cm⁻²·min⁻¹, concurring with a reduction of mean t_{sk} from 30.8 to 28.6 °C (Figure 8). As similar values of local skin temperature had been measured underneath bicycle helmets (De Bruyne et al., 2008; De Bruyne et al., 2012; Mukunthan et al., 2019), we used predicted mean t_{sk} as input to Eq. 6 for calculating head skin wettedness (w_{head}) depending on wind speed. The right panel of Figure 8 presents the results for SUD1 and SUD5 as the local sweat rate models based on sudomotor sensitivity with the lowest overall rmse (Figure 4), and for GSR2 representing models based on the LSR/GSR ratio, in relation to helmet evaporative resistance ($R_{et,head}$).

The vertical reference lines in the right panel of Figure 8 mark the upper $R_{et,head}$ threshold for maintaining head thermal comfort under low and high wind conditions, respectively. This will allow for benchmarking the evaporative resistance of the bicycle helmets, which are here indicated by the corresponding predicted values with 95% prediction intervals according to the regression function presented in Figure 6.

While for GSR2, the predicted local sweat rates and skin wettedness decreased with increasing air velocity due to the lower GSR predicted for $v_a = 6$ m·s⁻¹, the opposite effect was observed for SUD1 and SUD5 showing higher w_{head} for higher wind speed. This unexpected result could be explained by almost identical local sweat rates predicted by SUD for low and high wind conditions due to an almost identical predicted Δt_{re} in connection with a reduced evaporative capacity (E_{max} , Eq. 5) because of the lower saturated skin vapour pressure associated with the reduced t_{sk} (Eq. 6) under high wind.

Consequently, the upper $R_{et,head}$ threshold to maintain thermal comfort will unexpectedly decrease at high wind speed according to the predictions of SUD1 and SUD5, and would only be met according to SUD5 for helmets representing the lower end of the 95% prediction interval, i.e. for helmet designs optimized for evaporative cooling. In contrast, thermal comfort in a commuter scenario might not be obtainable according to SUD1. On the other hand, with GSR2 predicting lowered LSR resulting in lower w_{head} under high wind compared

to low wind conditions, thermal comfort might be achievable for less optimized helmets according to this model. Thus, thermal comfort will most probably be attainable for bicycle helmet use under the simulated conditions according to SUD5 and GSR2, but not according SUD1, for commuters with $v_a = 6 \text{ m}\cdot\text{s}^{-1}$. For the (somewhat artificial) situation with lower wind speed, the simulations indicated thermal discomfort in any case.

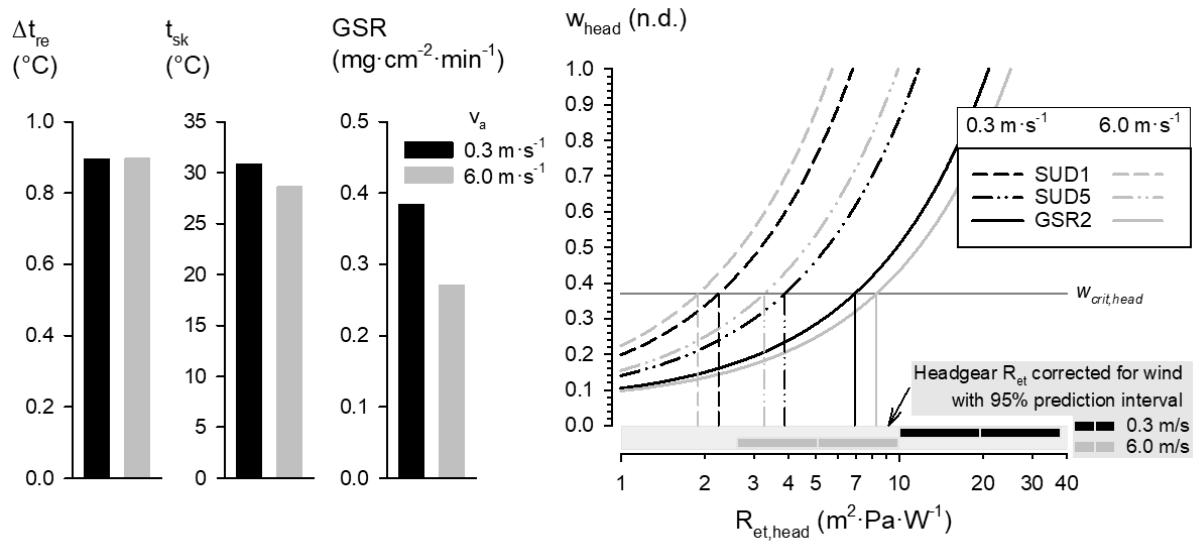


Figure 8. Core temperature increase (Δt_{re}), mean skin temperature (t_{sk}) and whole body gross sweat rate (GSR) predicted by the UTCI-Fiala model for the commuter cycling scenario with low and high relative air velocities (v_a), and resulting head skin wettedness (w_{head}) in relation to headgear evaporative resistance ($R_{et,head}$). Vertical reference lines indicate the upper limit of $R_{et,head}$ for maintaining w_{head} below the skin wettedness comfort limit $w_{crit,head}$. Corrections for the effect of v_a on $R_{et,head}$ with 95% prediction intervals were calculated as in Figure 6 using the regression coefficients from Table 5.

4 Discussion

4.1 Modelling framework

This study demonstrated how information on sudomotor sensitivities or on LSR/GSR ratios coupled with a model of human thermoregulation provides a basis to predict local sweat rates at the head (and at other body parts) concerning the characteristics of the thermal environment, activity level, clothing, and exposure duration. In connection with local skin wettedness calculation related to headgear evaporative resistance under use conditions, a modelling framework for the assessment the thermal comfort of bicycle helmet use in moderate to warm environments was established.

The study revealed a poor prediction of frontal *LSR*, especially by the local models relying on sudomotor sensitivity exhibiting considerable overestimation error. This might be related to insufficient consideration of convective cooling effects, which are highly influential in cycling activities and might modify the local sweating response (Nadel et al., 1971). In addition, there was a substantial spread in *LSR* predicted by different local models, mainly derived in studies under steady-state conditions with only a few participants. This variation in local model coefficients may thus partly reflect inter-individual variability, as a ten-fold increase from the lowest to highest sweating sensitivity at the forehead was observed between the ten participants in one experiment (Machado-Moreira et al., 2008b).

Although only limited published data were available for validation, they showed that models using sudomotor sensitivities derived from experiments with a similar workload as the validation data were superior to those from lower activity levels, e.g. SUD 5 vs. SUD 6 (Taylor and Machado-Moreira, 2013) or higher workloads, e.g. SUD 2 vs. SUD 3 (Smith and Havenith, 2011). Notably, SUD1 and SUD5, which exhibited the lowest overall rmse prediction error, were derived with cycling participants, i.e. using the same exercise mode as the validation experiments. The results also suggest that assuming a homogeneous sweating sensitivity (GSR1, i.e. $LSR=GSR$) gives inferior predictions compared to models considering regional differences (GSR2, GSR3).

In addition, there was a significant structural difference between the local models and the experimental data. The highest sweat rates were recorded at the medial head region with an unshaved scalp underneath a bicycle helmet, whereas the models all suggest the lowest sweat rates occurring at this side. The measurement of local sweat rates at shaved heads and thus unobstructed evaporation under low wind conditions used for model development in contrast to the experiments with increased air velocity $v_a=3\text{ m}\cdot\text{s}^{-1}$ under bicycle helmet use conditions may be one explanation for this discrepancy. This will also explain the lowest sweat rates observed at the frontal head, the region most exposed to wind in the experiments, in contrast to the highest sweat rates expected at the forehead according to most local models (Table 2).

Variance component analysis (Figure 3b) and summary statistics of the prediction error (Figure 4) did only suggest a slight influence of the chosen whole-body model on prediction accuracy. Nevertheless, it should be noted that the validation study was performed with

lightly clothed, moderately exercising subjects under steady climatic conditions. The PHS model was validated for predominantly steady-state conditions (Malchaire et al., 2001) and showed comparable results with the UTCI-Fiala model under such settings (Bröde et al., 2018). On the other hand, greater deviations from experimental data had been reported for the PHS when compared to advanced models under temporal changing, i.e. dynamic workloads or climatic conditions and with protective clothing exhibiting higher thermal insulation and evaporative resistance (Bröde et al., 2018; Lundgren-Kownacki et al., 2017; Wang et al., 2011). In addition, the wind speed of $3 \text{ m}\cdot\text{s}^{-1}$ applied in the validation study (cf. section 2.3) constitutes the upper limit of the range of validity for the PHS model (ISO 7933, 2004). In contrast, the advanced models (Fiala and Havenith, 2016; Fiala et al., 2012) have been studied and validated in a wide range of thermal and clothing conditions (Psikuta et al., 2012; Pokorný et al., 2017) including wind chill with very high air velocities (Ben Shabat et al., 2014; Bröde et al., 2013). Thus, modelling the commuter-cycling scenario with cycling at $6 \text{ m}\cdot\text{s}^{-1}$ was not possible with PHS, while being straightforward with UTCI-Fiala or FPC.

The high correlation of local sweating sensitivity (Smith and Havenith, 2011) with local skin wettedness comfort limits (Fukazawa and Havenith, 2009) as presented in Figure 5, suggests that comfort thresholds will be elevated in regions where more sweat is produced. Although the relation from Figure 5 is only supported by few body regions due to data scarcity and will require future verification, this finding is supported by higher whole-body threshold values reported for increasing activity levels associated with higher whole-body sweat rates (Fukazawa and Havenith, 2009; Gerrett et al., 2013; Gonzalez and Gagge, 1973).

Therefore, the outcome of the use case scenario indicating increasing skin wettedness associated with higher wind speed appears counterintuitive and points to a structural deficit of the local sweat rate models based on sudomotor sensitivity and, thus, on the change in body core temperature alone. Whether these models could be enhanced by considering the influence of (local) skin temperature (Nadel et al., 1971) may be a subject for future research. Notably, the models based on the LSR/GSR ratio did not suffer from this inconsistency.

The outcome of the simulated commuter cycling scenario emphasizes the necessity to evaluate the thermal properties of personal protective equipment under use conditions (DIN EN 17558:2020-11-Draft, 2020), in the case of bicycle helmets considering the wind effects

of relative air movements due to cycling speed reducing the thermal insulation and evaporative resistance at the head (and other body parts) substantially.

4.2 Research needs

The scarcity of data on human head perspiration, especially concerning bicycle helmet use conditions, implied that certain assumptions were required during modelling. Thus, more data-generating studies for model improvement and validation are imperative. More specifically, there is a need for:

- The improvement of local head sweating models, e.g. by considering the modifying effect of local skin temperature on sweating under convective cooling (Nadel et al., 1971).
- Biophysical testing of helmet's thermal insulation and evaporative resistance under still air conditions using head-forms and thermal manikins. Following the examples for clothing ensembles (ISO 9920, 2007) or local air layer evaporative resistance (Wang et al., 2012), further studies should be conducted with increased v_a for improving the correction equations predicting the reduction of the headgear thermal and evaporative resistances due to the forced convection induced by the cyclist's motion.
- Human trials comprising the measurement of head sweat rates and skin temperatures and their relation to skin wettedness and thermal comfort perception under bicycle helmet use conditions. Special attention should be paid to the effects of solar radiation, where appropriate helmet design might reduce the heat gain from sun irradiation (Bogerd et al., 2008; Brühwiler, 2008). This will allow for experimentally deriving relevant head skin wettedness comfort thresholds $w_{crit,head}$. These should be complemented by concurrent measurements of GSR and Δt_{re} besides LSR , thus facilitating the specific validation of the local models without employing whole-body thermoregulatory models. In particular, the number of female participants in such experiments urgently needs to be increased.

4.3 Future Developments

Finally, it should be noted that the principles presented here are easily transferable to consider local thermal comfort related to sweating at a still more detailed level, e.g. at the forehead or scalp, and at other body regions as necessary for optimizing sport clothes (Raccuglia et al., 2018b; Smith and Havenith, 2011) or footwear (Smith et al., 2013; West et al., 2019). Future developments towards more complete simulation tools may link this work with numerical approaches to modelling the heat and mass transport processes across the materials in contact with the skin (Mayor et al., 2015) or with integrated sensors for dynamic thermal comfort optimization (Youssef et al., 2019). This could enable a simultaneous investigation of further ergonomics issues, e.g. by integrating advanced anthropometric models (Lacko et al., 2015) for optimizing helmet fit and reducing complaints on head pressure, and, at the same time, ensuring non-compromised head impact protection modelled by finite element techniques (Bourdet et al., 2012; Deck et al., 2019; Fahlstedt et al., 2015).

5 Conclusions

The proposed modelling framework will enable for simulating, predicting and assessing the local thermal discomfort under bicycle helmet use conditions incorporating the (potentially time-varying) parameters of the thermal environment, exposure duration, activity level, clothing characteristics, and helmet's thermal properties.

By adding more experimental studies under use conditions for improving the accuracy and the spatial resolution of the comfort criteria, this modelling approach may evolve into a valuable tool for designers to adequately optimize the thermal properties of bicycle helmets, e.g. by novel materials (Venugopal et al., 2022) or improved ventilation and design solutions (Bandmann et al., 2018; De Bruyne et al., 2012; Kuklane et al., 2015), and enhancing the thermal comfort when wearing bicycle helmets.

In addition, we believe that the data on human head sweating underneath a bicycle helmet, recorded under realistic conditions from unshaved scalps, and concerning the wind effects on headgear thermal properties delivered by this study, together with the introduced framework, will form essential components contributing to the local thermal comfort assessment related to bicycle helmet use by digital human modelling in an emerging 'virtual ergonomics' context.

6 Acknowledgements

This work was funded as European Union COST Action TU1101 “Towards safer bicycling through optimization of bicycle helmets and usage”, also known as HOPE–Helmet Optimisation in Europe (<https://www.bicycle-helmets.eu>). We gratefully acknowledge the fruitful collaboration and contributions by our colleagues from Working Group 4 “Ergonomics of thermal effects”, as well as the support by the COST Office. COST was supported by the EU Framework Programme Horizon 2020.

6.1 Author contributions

Conceptualization: PB; Data curation: JMA, GDB, KK, PB; Formal analysis: PB; Investigation: KK, PB, TSM; Methodology: PB; Project administration: SA, JMA, PB, TSM; Resources: JMA, GDB, KK; Software: DF, TSM, PB; Visualization: PB; Roles/Writing - original draft: PB; Writing - review & editing: JMA, GDB, TSM, SA, KK, DF

6.2 Data Statement

All data used in this study are included either in the main text or in the appendix.

7 References

- Alfrey, E.J., Tracy, M., Alfrey, J.R., Carroll, M., Aranda-Wikman, E.D., Arora, T., Maa, J., Minnis, J., 2021. Helmet Usage Reduces Serious Head Injury Without Decreasing Concussion After Bicycle Riders Crash. *Journal of Surgical Research* 257, 593-596, <https://doi.org/10.1016/j.jss.2020.08.009>.
- Aljaste, H., Kuklane, K., Heidmets, S., COST Action TU1101 WG4, 2014. Better Bicycle Helmets for Commuters – Evaluation of Ventilation, International Cycling Safety Conference 2014. SAFER, Gothenburg, Sweden, pp. 1-7.
- Aljaste, H., Kuklane, K., Heidmets, S.S., 2015. The effects of air channel construction and design elements on heat transfer characteristics of bicycle helmets for commuters, in: Otte, D. (Ed.), 4th International Cycling Safety Conference. Medizinische Hochschule Hannover, Hannover, Germany, p. 8pp, <http://portal.research.lu.se/portal/files/5464732/7866945.pdf> (accessed 2022-10-14).
- Annaheim, S., Aerts, J.M., Bröde, P., De Bruyne, G., Flouris, A.D., Hursa Sajatovic, A., Kuklane, K., Martinez, N., Sotto Mayor, T., Bogerd, C.P., 2015. Final report of Working Group 4: Ergonomics of thermal effects, Brussels, Belgium, pp. 1-75, <http://publications.tno.nl/publication/34618505/rNiSjW> (accessed 2022-11-30).
- Bandmann, C.E.M., Akrami, M., Javadi, A.A., 2018. An investigation into the thermal comfort of a conceptual helmet model using finite element analysis and 3D computational fluid dynamics. *International Journal of Industrial Ergonomics* 68, 125-136, <https://doi.org/10.1016/j.ergon.2018.07.004>.

- Ben Shabat, Y., Shitzer, A., Fiala, D., 2014. Modified wind chill temperatures determined by a whole body thermoregulation model and human-based facial convective coefficients. *International Journal of Biometeorology* 58, 1007-1015, <https://doi.org/10.1007/s00484-013-0698-z>.
- Berlin, C., Kajaks, T., 2010. Time-related ergonomics evaluation for DHMs: a literature review. *International Journal of Human Factors Modelling and Simulation* 1, 356-379, <https://doi.org/10.1504/ijhfms.2010.040271>.
- Bogerd, C.P., 2011. Memorandum of Understanding for the implementation of a European Concerted Research Action designated as COST Action TU1101: Towards safer bicycling through optimization of bicycle helmets and usage. COST Office, Bruxelles, https://e-services.cost.eu/files/domain_files/TUD/Action_TU1101/mou/TU1101-e.pdf (accessed 2022-09-30).
- Bogerd, C.P., Aerts, J.M., Annaheim, S., Bröde, P., De Bruyne, G., Flouris, A.D., Kuklane, K., Sotto Mayor, T., Rossi, R.M., 2015a. A review on ergonomics of headgear: Thermal effects. *International Journal of Industrial Ergonomics* 45, 1-12, <https://doi.org/10.1016/j.ergon.2014.10.004>.
- Bogerd, C.P., Annaheim, S., Halldin, P., Houtenbos, M., Otte, D., Shinar, D., Walker, I., Willinger, R., 2015b. Helmet Optimization in Europe: The final report of COST Action TU1101 / HOPE, Brussels, Belgium, pp. 1-45, <http://publications.tno.nl/publication/34618446/7HCUzO> (accessed 2022-09-30).
- Bogerd, C.P., Brühwiler, P.A., Heus, R., 2008. The effect of rowing headgear on forced convective heat loss and radiant heat gain on a thermal manikin headform. *Journal of Sports Sciences* 26, 733-741, <https://doi.org/10.1080/02640410701787783>.
- Borman, I., 2016. Digitizelt - Plot Digitizer Software. Digitize graphs, charts and math data, <https://www.digitizeit.xyz/> (accessed 2022-10-14).
- Bourdet, N., Deck, C., Carreira, R.P., Willinger, R., 2012. Head impact conditions in the case of cyclist falls. *Proceedings of the Institution of Mechanical Engineers, Part P: Journal of Sports Engineering and Technology* 226, 282-289, <https://doi.org/10.1177/1754337112442326>.
- Bröde, P., Blazejczyk, K., Fiala, D., Havenith, G., Holmér, I., Jendritzky, G., Kuklane, K., Kampmann, B., 2013. The Universal Thermal Climate Index UTCI Compared to Ergonomics Standards for Assessing the Thermal Environment. *Industrial Health* 51, 16-24, <https://doi.org/10.2486/indhealth.2012-0098>.
- Bröde, P., Fiala, D., Blazejczyk, K., Holmér, I., Jendritzky, G., Kampmann, B., Tinz, B., Havenith, G., 2012. Deriving the operational procedure for the Universal Thermal Climate Index (UTCI). *International Journal of Biometeorology* 56, 481-494, <https://doi.org/10.1007/s00484-011-0454-1>.
- Bröde, P., Fiala, D., Lemke, B., Kjellstrom, T., 2018. Estimated work ability in warm outdoor environments depends on the chosen heat stress assessment metric. *International Journal of Biometeorology* 62, 331-345, <https://doi.org/10.1007/s00484-017-1346-9>.
- Brühwiler, P.A., 2003. Heated, perspiring manikin headform for the measurement of headgear ventilation characteristics. *Measurement Science and Technology* 14, 217-227, <https://doi.org/10.1088/0957-0233/14/2/309>.
- Brühwiler, P.A., 2008. Radiant heat transfer of bicycle helmets and visors. *Journal of Sports Sciences* 26, 1025-1031, <https://doi.org/10.1080/02640410801930143>.

- Brühwiler, P.A., Buyan, M., Huber, R., Bogerd, C.P., Sznitman, J., Graf, S.F., Rösger, T., 2006. Heat transfer variations of bicycle helmets. *Journal of Sports Sciences* 24, 999-1011, <https://doi.org/10.1080/02640410500457877>.
- Chen, H., Mullet, K., Cluver, B., 2006. Evaluation of Military Ballistic Helmets Using a Thermal Manikin, in: Fan, J. (Ed.), *Sixth International Thermal Manikin and Modeling Meeting (6I3M)*. The Hong Kong Polytechnic University, Hong Kong, pp. 330-335.
- D'Ambrosio Alfano, F.R., Palella, B.I., Riccio, G., Malchaire, J., 2016. On the Effect of Thermophysical Properties of Clothing on the Heat Strain Predicted by PHS Model. *Annals of Occupational Hygiene* 60, 231-251, <https://doi.org/10.1093/annhyg/mev070>.
- De Bruyne, G., Aerts, J.M., Sloten, J.V., Goffin, J., Verpoest, I., Berckmans, D., 2010. Transient sweat response of the human head during cycling. *International Journal of Industrial Ergonomics* 40, 406-413, <https://doi.org/10.1016/j.ergon.2010.02.005>.
- De Bruyne, G., Aerts, J.M., Van der Perre, G., Goffin, J., Verpoest, I., Berckmans, D., 2008. Spatial differences in sensible and latent heat losses under a bicycle helmet. *European Journal of Applied Physiology* 104, 719-726, <https://doi.org/10.1007/s00421-008-0828-1>.
- De Bruyne, G., Aerts, J.M., Vander Sloten, J., Goffin, J., Verpoest, I., Berckmans, D., 2012. Quantification of local ventilation efficiency under bicycle helmets. *International Journal of Industrial Ergonomics* 42, 278-286, <https://doi.org/10.1016/j.ergon.2012.02.003>.
- de Geus, B., De Smet, S., Nijs, J., Meeusen, R., 2007. Determining the intensity and energy expenditure during commuter cycling. *British Journal of Sports Medicine* 41, 8-12, <https://doi.org/10.1136/bjsm.2006.027615>.
- Deck, C., Bourdet, N., Meyer, F., Willinger, R., 2019. Protection performance of bicycle helmets. *Journal of Safety Research* 71, 67-77, <https://doi.org/10.1016/j.jsr.2019.09.003>.
- DIN EN 17558:2020-11-Draft, 2020. *Ergonomics - Ergonomics of PPE ensembles; German and English version prEN 17558:2020*. Beuth Verlag, Berlin, <https://doi.org/10.31030/3178798>.
- Dotti, F., Ferri, A., Moncalero, M., Colonna, M., 2016. Thermo-physiological comfort of soft-shell back protectors under controlled environmental conditions. *Applied Ergonomics* 56, 144-152, <https://doi.org/10.1016/j.apergo.2016.04.002>.
- Ettema, G., Loras, H.W., 2009. Efficiency in cycling: a review. *European Journal of Applied Physiology* 106, 1-14, <https://doi.org/10.1007/s00421-009-1008-7>.
- European Commission, 2012. Standardization mandate in the field of protective textiles and personal protective clothing and equipment, M/509 EN, Brussels, <https://www.cenelec.eu/media/CEN-CENELEC/Areas%20of%20Work/CEN-CENELEC%20Topics/PPE/Quicklinks%20General/European%20Legislation/m509.pdf> (accessed 2022-10-14).
- Evers, C., 2022. Gurte, Kindersitze, Helme und Schutzkleidung - 2021 [Safety belts, child seats, safety helmets and protective clothing - 2021], Daten und Fakten kompakt. Bundesanstalt für Straßenwesen, Bergisch Gladbach, <https://www.bast.de/DE/Publikationen/DaFa/2022-2021/2022-02.html> (accessed 2022-10-19).

- Fahlstedt, M., Depreitere, B., Halldin, P., Vander Sloten, J., Kleiven, S., 2015. Correlation between Injury Pattern and Finite Element Analysis in Biomechanical Reconstructions of Traumatic Brain Injuries. *Journal of Biomechanics* 48, 1331-1335, <https://doi.org/10.1016/j.jbiomech.2015.02.057>.
- Fanger, P.O., 1972. *Thermal Comfort*. McGraw-Hill Book Co, New York.
- Fiala, D., Havenith, G., 2016. Modelling Human Heat Transfer and Temperature Regulation, in: Gefen, A., Epstein, Y. (Eds.), *The Mechanobiology and Mechanophysiology of Military-Related Injuries*. Springer International Publishing, Cham, pp. 265-302, https://doi.org/10.1007/8415_2015_183.
- Fiala, D., Havenith, G., Bröde, P., Kampmann, B., Jendritzky, G., 2012. UTCI-Fiala multi-node model of human heat transfer and temperature regulation. *International Journal of Biometeorology* 56, 429-441, <https://doi.org/10.1007/s00484-011-0424-7>.
- Fiala, D., Psikuta, A., Jendritzky, G., Paulke, S., Nelson, D.A., van Marken Lichtenbelt, W., Frijns, A.J., 2010. Physiological modeling for technical, clinical and research applications. *Frontiers in Bioscience* S2, 939-968, <https://doi.org/10.2741/112>.
- Fojtlin, M., Psikuta, A., Fišer, J., Toma, R., Annaheim, S., Jicha, M., 2019. Local clothing properties for thermo-physiological modelling: Comparison of methods and body positions. *Building and Environment* 155, 376-388. <https://doi.org/10.1016/j.buildenv.2019.03.026>.
- Fonseca, G.F., 1974. Heat Transfer Properties of Military Protective Headgear, Natick, MA, pp. 1-32, <https://apps.dtic.mil/sti/pdfs/AD0783434.pdf> (accessed 2022-10-14).
- Fukazawa, T., Havenith, G., 2009. Differences in comfort perception in relation to local and whole body skin wettedness. *European Journal of Applied Physiology* 106, 15-24, <https://doi.org/10.1007/s00421-009-0983-z>.
- Gagge, A.P., 1937. A new physiological variable associated with sensible and insensible perspiration. *American Journal of Physiology* 120, 277-287, <http://ajplegacy.physiology.org/content/120/2/277.short>.
- Gagge, A.P., Stolwijk, J.A.J., Hardy, J.D., 1967. Comfort and thermal sensations and associated physiological responses at various ambient temperatures. *Environmental Research* 1, 1-20, [https://doi.org/10.1016/0013-9351\(67\)90002-3](https://doi.org/10.1016/0013-9351(67)90002-3).
- Gagge, A.P., Stolwijk, J.A.J., Saltin, B., 1969. Comfort and thermal sensations and associated physiological responses during exercise at various ambient temperatures. *Environmental Research* 2, 209-229, [https://doi.org/10.1016/0013-9351\(69\)90037-1](https://doi.org/10.1016/0013-9351(69)90037-1).
- Gerrett, N., Redortier, B., Voelcker, T., Havenith, G., 2013. A comparison of galvanic skin conductance and skin wettedness as indicators of thermal discomfort during moderate and high metabolic rates. *Journal of Thermal Biology* 38, 530-538, <https://doi.org/10.1016/j.jtherbio.2013.09.003>.
- Gonzalez, R.R., Gagge, A.P., 1973. Magnitude estimates of thermal discomfort during transients of humidity and operative temperature and their relation to the new ASHRAE Effective Temperature (ET*). *ASHRAE Transactions* 79, 88-96.
- Havenith, G., 2004. Thermal Conditions Measurement, in: Stanton, N., Hedge, A., Brookhuis, K., Salas, E., Hendrick, H. (Eds.), *Handbook of Human Factors and Ergonomics Methods*. CRC Press, Boca Raton, FA, pp. 60-61-60-16, <https://doi.org/10.1201/9780203489925.ch60>.

- Havenith, G., Fiala, D., 2016. Thermal Indices and Thermophysiological Modeling for Heat Stress. *Comprehensive Physiology* 6, 255-302, <https://doi.org/10.1002/cphy.c140051>.
- Havenith, G., Nilsson, H.O., 2004. Correction of clothing insulation for movement and wind effects, a meta-analysis. *Eur. J. Appl. Physiol* 92, 636-640, <https://doi.org/10.1007/s00421-004-1113-6>.
- Havenith, G., Nilsson, H.O., 2005. Erratum to: Correction of clothing insulation for movement and wind effects, a meta-analysis. *European Journal of Applied Physiology* 93, 506-506, <https://doi.org/10.1007/s00421-004-1267-2>.
- Havenith, G., Richards, M.G., Wang, X., Bröde, P., Candas, V., den Hartog, E., Holmér, I., Kuklane, K., Meinander, H., Nocker, W., 2008. Apparent latent heat of evaporation from clothing: attenuation and "heat pipe" effects. *Journal of Applied Physiology* 104, 142-149, <https://doi.org/10.1152/japplphysiol.00612.2007>.
- Holmér, I., 2006. Protective clothing in hot environments. *Ind Health* 44, 404-413, <https://doi.org/10.2486/indhealth.44.404>.
- Høye, A., 2018. Bicycle helmets – To wear or not to wear? A meta-analyses of the effects of bicycle helmets on injuries. *Accident Analysis & Prevention* 117, 85-97, <https://doi.org/10.1016/j.aap.2018.03.026>.
- ISO 7933, 2004. Ergonomics of the thermal environment - Analytical determination and interpretation of heat stress using calculation of the predicted heat strain. International Organisation for Standardisation, Geneva.
- ISO 9920, 2007. Ergonomics of the thermal environment - Estimation of thermal insulation and water vapour resistance of a clothing ensemble. International Organisation for Standardisation, Geneva.
- Kampmann, B., Bröde, P., Fiala, D., 2012. Physiological responses to temperature and humidity compared to the assessment by UTCI, WGBT and PHS. *International Journal of Biometeorology* 56, 505-513, <https://doi.org/10.1007/s00484-011-0410-0>.
- Kuklane, K., Aljaste, H., Heidmets, S.S., 2015. Better bicycle helmets for commuters: design solutions for ventilation, in: Annaheim, S., Aerts, J.M., Bröde, P., De Bruyne, G., Flouris, A.D., Hursa Sajatovic, A., Kuklane, K., Martinez, N., Sotto Mayor, T., Bogerd, C.P. (Eds.), *Final report of Working Group 4: Ergonomics of thermal effects. COST Action TU1101 / HOPE*, Brussels, Belgium, pp. 41-67, <http://publications.tno.nl/publication/34618505/rNiSjW> (accessed 2022-10-14).
- Kuklane, K., Eggeling, J., Kemmeren, M., Heus, R., 2022. A Database of Static Thermal Insulation and Evaporative Resistance Values of Dutch Firefighter Clothing Items and Ensembles. *Biology* 11, 1813, <https://doi.org/10.3390/biology11121813>.
- Lacko, D., Huysmans, T., Parizel, P.M., De Bruyne, G., Verwulgen, S., Van Hulle, M.M., Sijbers, J., 2015. Evaluation of an anthropometric shape model of the human scalp. *Applied Ergonomics* 48, 70-85, <https://doi.org/10.1016/j.apergo.2014.11.008>.
- Lanzotti, A., Vanacore, A., Tarallo, A., Nathan-Roberts, D., Coccorese, D., Minopoli, V., Carbone, F., d'Angelo, R., Grasso, C., Di Gironimo, G., Papa, S., 2020. Interactive tools for safety 4.0: virtual ergonomics and serious games in real working contexts. *Ergonomics* 63, 324-333, <https://doi.org/10.1080/00140139.2019.1683603>.

- Ledesma, R.D., Shinar, D., Valero-Mora, P.M., Haworth, N., Ferraro, O.E., Morandi, A., Papadakaki, M., De Bruyne, G., Otte, D., Saplioglu, M., 2019. Psychosocial factors associated with helmet use by adult cyclists. *Transportation Research Part F: Traffic Psychology and Behaviour* 65, 376-388, <https://doi.org/10.1016/j.trf.2019.08.003>.
- Littell, R.C., Milliken, G.A., Stroup, W.W., Wolfinger, R.D., Schabenberger, O., 2006. *SAS® System for Mixed Models*, Second Edition. SAS Institute Inc., Cary, NC.
- Liu, X., Holmér, I., 1995. Evaporative heat transfer characteristics of industrial safety helmets. *Applied Ergonomics* 26, 135-140, [https://doi.org/10.1016/0003-6870\(95\)00010-A](https://doi.org/10.1016/0003-6870(95)00010-A).
- Liu, X., Holmér, I., 1997. Evaluation of Evaporative Heat Transfer Characteristics of Helmets. *Applied Human Science* 16, 107-113, <https://doi.org/10.2114/jpa.16.107>.
- Lu, Y., Wang, F., Wan, X., Song, G., Zhang, C., Shi, W., 2015. Clothing resultant thermal insulation determined on a movable thermal manikin. Part II: effects of wind and body movement on local insulation. *International Journal of Biometeorology* 59, 1487-1498, <https://doi.org/10.1007/s00484-015-0959-0>.
- Lundgren-Kownacki, K., Martínez, N., Johansson, B., Psikuta, A., Annaheim, S., Kuklane, K., 2017. Human responses in heat – comparison of the Predicted Heat Strain and the Fiala multi-node model for a case of intermittent work. *Journal of Thermal Biology* 70, 45-52, <https://doi.org/10.1016/j.jtherbio.2017.05.006>.
- Machado-Moreira, C., Smith, F., van den Heuvel, A., Mekjavic, I., Taylor, N., 2008a. Sweat secretion from the torso during passively-induced and exercise-related hyperthermia. *European Journal of Applied Physiology* 104, 265-270, <https://doi.org/10.1007/s00421-007-0646-x>.
- Machado-Moreira, C., Wilmsink, F., Meijer, A., Mekjavic, I., Taylor, N., 2008b. Local differences in sweat secretion from the head during rest and exercise in the heat. *European Journal of Applied Physiology* 104, 257-264, <https://doi.org/10.1007/s00421-007-0645-y>.
- Malchaire, J., Piette, A., 2004. Predicted Heat Strain (PHS) model computation programme written in Quick Basic: exact copy of the programme of annex D of the ISO 7933, <http://www.deparisnet.be/chaleur/Normes/iso7933n.pdf> (accessed 2015-08-27).
- Malchaire, J., Piette, A., Kampmann, B., Mehnert, P., Gebhardt, H., Havenith, G., den Hartog, E.A., Holmér, I., Parsons, K., Alfano, G., Griefahn, B., 2001. Development and validation of the predicted heat strain model. *Ann Occup Hyg* 45, 123-135, <http://www.ncbi.nlm.nih.gov/pubmed/11182426>.
- Martinez, N., 2016. Multi-sector thermophysiological head simulator for headgear research, Universitat Politècnica de València, Valencia, Spain, <https://doi.org/10.4995/Thesis/10251/61487>.
- Martínez, N., Psikuta, A., Rossi, R.M., Corberán, J.M., Annaheim, S., 2016. Global and local heat transfer analysis for bicycle helmets using thermal head manikins. *International Journal of Industrial Ergonomics* 53, 157-166, <https://doi.org/10.1016/j.ergon.2015.11.012>.
- Mayor, T.S., Couto, S., Psikuta, A., Rossi, R.M., 2015. Advanced modelling of the transport phenomena across horizontal clothing microclimates with natural convection. *International Journal of Biometeorology* 59, 1875-1889, <https://doi.org/10.1007/s00484-015-0994-x>.

- Morris, N.B., Cramer, M.N., Hodder, S.G., Havenith, G., Jay, O., 2013. A comparison between the technical absorbent and ventilated capsule methods for measuring local sweat rate. *Journal of Applied Physiology* 114, 816-823, <https://doi.org/10.1152/jappphysiol.01088.2012>.
- Mukunthan, S., Vleugels, J., Huysmans, T., Kuklane, K., Mayor, T.S., De Bruyne, G., 2019. Thermal-Performance Evaluation of Bicycle Helmets for Convective and Evaporative Heat Loss at Low and Moderate Cycling Speeds. *Applied Sciences* 9, 3672, <https://doi.org/10.3390/app9183672>.
- Nadel, E.R., Bullard, R.W., Stolwijk, J.A., 1971. Importance of skin temperature in the regulation of sweating. *Journal of Applied Physiology* 31, 80-87, <https://doi.org/10.1152/jappl.1971.31.1.80>.
- Nilsson, H.O., 2007. Thermal comfort evaluation with virtual manikin methods. *Building and Environment* 42, 4000-4005, <https://doi.org/10.1016/j.buildenv.2006.04.027>.
- Otte, D., Jänsch, M., Chliaoutakis, J., Tzamalouka, G., Morandi, A., Orsi, C., Pereira-Dias, J.M., 2014. Cyclist-reported habits of helmet usage in Europe and differences in riding positions by using helmets, 3rd International Cycling Safety Conference (ICSC2014). SAFER, Gothenburg, Sweden, p. 2pp.
- Otte, D., Jänsch, M., Morandi, A., Orsi, C., Stendardo, A., Bogerd, C.P., Tzamalouca, G., Papadakaki, M., Chliaoutakis, J., Parkkari, K., Dias, J., Weber, T., 2015. Final report of Working Group 1: In-depth accident observations and injury statistics, Brussels, Belgium, pp. 1-69, <http://publications.tno.nl/publication/34618467/2IAaBQ> (accessed 2022-09-30).
- Pang, T.Y., Subic, A., Takla, M., 2014. Evaluation of thermal and evaporative resistances in cricket helmets using a sweating manikin. *Applied Ergonomics* 45, 300-307, <https://doi.org/10.1016/j.apergo.2013.04.011>.
- Parsons, K.C., 2014. *Human Thermal Environments: The Effects of Hot, Moderate and Cold Environments on Human Health, Comfort and Performance*, 3rd ed. CRC Press, London.
- Paul, G., Wischniewski, S., 2012. Standardisation of digital human models. *Ergonomics* 55, 1115-1118, <https://doi.org/10.1080/00140139.2012.690454>.
- Pokorný, J., Fišer, J., Fojtlín, M., Kopečková, B., Toma, R., Slabotínský, J., Jícha, M., 2017. Verification of Fiala-based human thermophysiological model and its application to protective clothing under high metabolic rates. *Building and Environment* 126, 13-26, <https://doi.org/10.1016/j.buildenv.2017.08.017>.
- Psikuta, A., Fiala, D., Laschewski, G., Jendritzky, G., Richards, M., Blazejczyk, K., Mekjavic, I.B., Rintamäki, H., de Dear, R., Havenith, G., 2012. Validation of the Fiala multi-node thermophysiological model for UTCI application. *International Journal of Biometeorology* 56, 443-460, <https://doi.org/10.1007/s00484-011-0450-5>.
- Psikuta, A., Kuklane, K., Bogdan, A., Havenith, G., Annaheim, S., Rossi, R.M., 2016. Opportunities and constraints of presently used thermal manikins for thermo-physiological simulation of the human body. *International Journal of Biometeorology* 60, 435-446, <https://doi.org/10.1007/s00484-015-1041-7>.
- Raccuglia, M., Heyde, C., Lloyd, A., Hodder, S., Havenith, G., 2018a. Spatial and temporal migration of sweat: from skin to clothing. *European Journal of Applied Physiology*, <https://doi.org/10.1007/s00421-018-3941-9>.

Raccuglia, M., Sales, B., Heyde, C., Havenith, G., Hodder, S., 2018b. Clothing comfort during physical exercise – Determining the critical factors. *Applied Ergonomics* 73, 33-41, <https://doi.org/10.1016/j.apergo.2018.05.014>.

Rakap, S., Rakap, S., Evran, D., Cig, O., 2016. Comparative evaluation of the reliability and validity of three data extraction programs: UnGraph, GraphClick, and Digitizelt. *Computers in Human Behavior* 55, 159-166, <https://doi.org/10.1016/j.chb.2015.09.008>.

Shinar, D., Valero-Mora, P., van Strijp-Houtenbos, M., Haworth, N., Schramm, A., De Bruyne, G., Cavallo, V., Chliaoutakis, J., Dias, J., Ferraro, O.E., Fyhri, A., Sajatovic, A.H., Kuklane, K., Ledesma, R., Mascarell, O., Morandi, A., Muser, M., Otte, D., Papadakaki, M., Sanmartín, J., Dulf, D., Saplioglu, M., Tzamalouka, G., 2018. Under-reporting bicycle accidents to police in the COST TU1101 international survey: Cross-country comparisons and associated factors. *Accident Analysis & Prevention* 110, 177-186, <https://doi.org/10.1016/j.aap.2017.09.018>.

Smallcombe, J., Hodder, S., Loveday, D., Kuklane, K., Mlynarczyk, M., Halder, A., Petersson, J., Havenith, G., 2021. Updated database of clothing thermal insulation and vapor permeability values of western ensembles for use in ASHRAE standard 55, ISO 7730 and ISO 9920; Results of ASHRAE RP-1760. *ASHRAE Transactions* 121, 773-799.

Smith, C.J., Havenith, G., 2011. Body mapping of sweating patterns in male athletes in mild exercise-induced hyperthermia. *European Journal of Applied Physiology* 111, 1391-1404, <https://doi.org/10.1007/s00421-010-1744-8>.

Smith, C.J., Machado-Moreira, C.A., Plant, G., Hodder, S.G., Havenith, G., Taylor, N.A.S., 2013. Design data for footwear: sweating distribution on the human foot. *International Journal of Clothing Science and Technology* 25, 43-58, <https://doi.org/10.1108/09556221311292200>.

Taylor, N.A.S., Caldwell, J.N., Mekjavic, I.B., 2006. The Sweating Foot: Local Differences in Sweat Secretion During Exercise-Induced Hyperthermia. *Aviation, Space, and Environmental Medicine* 77, 1020-1027.

Taylor, N.A.S., Machado-Moreira, C.A., 2011. Regional variations in sweat gland density, insensible and thermal perspiration, and the electrolyte composition of sweat: physiologists, modellers, engineers, lend us your ears, in: Kounalakis, S.N., Koskolou, M. (Eds.), 14th International Conference on Environmental Ergonomics. National and Kapodestrian University of Athens, Nafplio, Greece, pp. 136-139.

Taylor, N.A.S., Machado-Moreira, C.A., 2013. Regional variations in transepidermal water loss, eccrine sweat gland density, sweat secretion rates and electrolyte composition in resting and exercising humans. *Extreme Physiology & Medicine* 2, 4, <https://doi.org/10.1186/2046-7648-2-4>.

Ueda, H., Inoue, Y., Matsudaira, M., Araki, T., Havenith, G., 2006. Regional microclimate humidity of clothing during light work as a result of the interaction between local sweat production and ventilation. *International Journal of Clothing Science and Technology* 18, 225-234, <https://doi.org/10.1108/09556220610668473>.

Ueno, S., Sawada, S.-i., 2019. Effects of ventilation openings in industrial safety helmets on evaporative heat dissipation. *Journal of Occupational Health* 61, 157-164, <https://doi.org/10.1002/1348-9585.12024>.

- Vargas, N.T., Chapman, C.L., Ji, W., Johnson, B.D., Gathercole, R., Schlader, Z.J., 2020. Increased skin wetness independently augments cool-seeking behaviour during passive heat stress. *The Journal of Physiology* 598, 2775-2790, <https://doi.org/10.1113/jp279537>.
- Varriano, B., Porplycia, D., Friedman, S.M., 2022. Unhelmeted Injured Cyclists in a Canadian Emergency Department: Cycling Behavior and Attitudes Towards Helmet Use. *INQUIRY: The Journal of Health Care Organization, Provision, and Financing* 59, 00469580221083276, <https://doi.org/10.1177/00469580221083276>.
- Venugopal, A., Anzil, K.K., Thomas, B.G., Varghese, J.T., 2022. Nano-enhanced phase change material for thermal comfort at skull and environment interface in riding helmets: An experimental investigation. *Journal of Energy Storage* 50, 104332, <https://doi.org/10.1016/j.est.2022.104332>.
- Wang, F., del Ferraro, S., Lin, L.Y., Sotto Mayor, T., Molinaro, V., Ribeiro, M., Gao, C., Kuklane, K., Holmér, I., 2012. Localised boundary air layer and clothing evaporative resistances for individual body segments. *Ergonomics* 55, 799-812, <https://doi.org/10.1080/00140139.2012.668948>.
- Wang, F., Kuklane, K., Gao, C., Holmér, I., 2011. Can the PHS model (ISO7933) predict reasonable thermophysiological responses while wearing protective clothing in hot environments? *Physiological Measurement* 32, 239, <https://doi.org/10.1088/0967-3334/32/2/007>.
- West, A.M., Tarrier, J., Hodder, S., Havenith, G., 2019. Sweat distribution and perceived wetness across the human foot: the effect of shoes and exercise intensity. *Ergonomics* 62, 1450-1461, <https://doi.org/10.1080/00140139.2019.1657185>.
- Youssef, A., Colon, J., Mantzios, K., Gkiata, P., Mayor, T.S., Flouris, A.D., De Bruyne, G., Aerts, J.-M., 2019. Towards Model-Based Online Monitoring of Cyclist's Head Thermal Comfort: Smart Helmet Concept and Prototype. *Applied Sciences* 9, 3170, <https://doi.org/10.3390/app9153170>.
- Zhang, H., Arens, E., Huizenga, C., Han, T., 2010a. Thermal sensation and comfort models for non-uniform and transient environments, part II: Local comfort of individual body parts. *Building and Environment* 45, 389-398, <https://doi.org/10.1016/j.buildenv.2009.06.015>.
- Zhang, H., Arens, E., Huizenga, C., Han, T., 2010b. Thermal sensation and comfort models for non-uniform and transient environments: Part I: Local sensation of individual body parts. *Building and Environment* 45, 380-388, <https://doi.org/10.1016/j.buildenv.2009.06.018>.
- Zwolinska, M., 2013. Thermal subjective sensations of motorcyclists. *Accident Analysis & Prevention* 50, 1211-1220, <https://doi.org/10.1016/j.aap.2012.09.021>.
- Zwolinska, M., Bogdan, A., Fejdys, M., 2014. Influence of different types of the internal system of the ballistic helmet shell on the thermal insulation measured by a manikin headform. *International Journal of Industrial Ergonomics* 44, 421-427, <https://doi.org/10.1016/j.ergon.2013.11.011>.

Appendix A: Datasets

This appendix provides the datasets used for validating LSR predictions against observed head sweat rates (Table A.1), and for deriving the correction equations for the effect of air velocity on thermal insulation and evaporation resistance of headgear (Table A.2) as well as of the boundary air layer around the nude head (Table A.3).

Table A.1. Local sweat rates observed (LSR_{obs}) at the frontal, lateral and medial head regions of 9 subjects (ID) performing up to three repetitions (Rep) of bicycle ergometer exercise following a gender specific low and high workload protocol while wearing a bicycle helmet (De Bruyne et al, 2008).

Head region	Workload	Gender	ID	Rep	LSR_{obs} ($mg \cdot cm^{-2} \cdot min^{-1}$)
frontal	low	female	4	1	0.521
frontal	low	female	4	2	0.381
frontal	low	female	6	1	0.778
frontal	low	female	6	2	0.142
frontal	low	female	7	1	0.413
frontal	low	female	9	1	0.103
frontal	low	female	9	2	1.074
frontal	low	female	9	3	1.190
frontal	low	male	1	1	0.541
frontal	low	male	1	2	0.422
frontal	low	male	1	3	0.846
frontal	low	male	2	1	0.350
frontal	low	male	2	2	0.450
frontal	low	male	2	3	0.193
frontal	low	male	3	1	1.798
frontal	low	male	3	2	0.626
frontal	low	male	5	1	0.229
frontal	low	male	5	2	0.459
frontal	low	male	5	3	0.625
frontal	low	male	8	1	0.057
frontal	low	male	8	2	0.429
frontal	low	male	8	3	0.586
frontal	high	female	4	1	0.791
frontal	high	female	4	2	0.745
frontal	high	female	6	1	0.663
frontal	high	female	6	2	0.329
frontal	high	female	9	1	0.603
frontal	high	female	9	2	1.482
frontal	high	female	9	3	1.719
frontal	high	male	1	1	2.735
frontal	high	male	1	2	1.588
frontal	high	male	1	3	1.246

<i>Head region</i>	<i>Workload</i>	<i>Gender</i>	<i>ID</i>	<i>Rep</i>	<i>LSR_{obs}</i> (<i>mg·cm⁻²·min⁻¹</i>)
frontal	high	male	2	1	0.760
frontal	high	male	2	2	1.155
frontal	high	male	2	3	0.622
frontal	high	male	3	1	2.558
frontal	high	male	3	3	2.289
frontal	high	male	5	1	0.859
frontal	high	male	5	2	0.972
frontal	high	male	5	3	0.641
frontal	high	male	8	1	0.461
frontal	high	male	8	2	1.067
frontal	high	male	8	3	1.437
lateral	low	female	4	1	0.365
lateral	low	female	4	2	0.388
lateral	low	female	6	1	0.621
lateral	low	female	6	2	0.047
lateral	low	female	7	1	0.382
lateral	low	female	9	1	0.034
lateral	low	female	9	2	1.150
lateral	low	female	9	3	0.707
lateral	low	male	1	1	0.209
lateral	low	male	1	2	0.293
lateral	low	male	1	3	0.711
lateral	low	male	2	1	0.268
lateral	low	male	2	2	0.374
lateral	low	male	2	3	0.114
lateral	low	male	3	1	1.678
lateral	low	male	3	2	1.003
lateral	low	male	3	3	2.212
lateral	low	male	5	1	0.209
lateral	low	male	5	2	0.299
lateral	low	male	5	3	0.703
lateral	low	male	8	1	0.032
lateral	low	male	8	2	0.467
lateral	low	male	8	3	0.561
lateral	high	female	4	1	0.547
lateral	high	female	4	2	0.581
lateral	high	female	6	1	0.473
lateral	high	female	6	2	0.302
lateral	high	female	7	1	0.753
lateral	high	female	9	1	0.706
lateral	high	female	9	2	1.741
lateral	high	female	9	3	1.933
lateral	high	male	1	1	0.601
lateral	high	male	1	2	0.833
lateral	high	male	1	3	2.241
lateral	high	male	2	1	0.700
lateral	high	male	2	2	0.697
lateral	high	male	2	3	0.378
lateral	high	male	3	1	2.869
lateral	high	male	3	2	3.414

<i>Head region</i>	<i>Workload</i>	<i>Gender</i>	<i>ID</i>	<i>Rep</i>	<i>LSR_{obs}</i> (<i>mg·cm⁻²·min⁻¹</i>)
lateral	high	male	3	3	2.958
lateral	high	male	5	1	0.794
lateral	high	male	5	2	0.733
lateral	high	male	5	3	1.070
lateral	high	male	8	1	0.567
lateral	high	male	8	2	0.976
lateral	high	male	8	3	1.625
medial	low	female	6	2	0.491
medial	low	male	1	1	-.019
medial	low	male	1	1	1.051
medial	low	male	1	2	-.056
medial	low	male	1	2	0.209
medial	low	male	1	3	0.461
medial	low	male	1	3	0.711
medial	low	male	2	1	1.049
medial	low	male	2	2	0.700
medial	low	male	2	3	0.230
medial	low	male	2	3	0.468
medial	low	male	5	1	1.020
medial	low	male	5	1	0.971
medial	low	male	5	2	1.478
medial	low	male	5	2	1.838
medial	low	male	5	3	2.372
medial	low	male	5	3	1.432
medial	low	male	8	1	0.028
medial	low	male	8	3	0.489
medial	low	male	8	3	0.576
medial	high	female	6	2	2.680
medial	high	male	1	1	0.370
medial	high	male	1	1	3.506
medial	high	male	1	2	2.390
medial	high	male	1	2	2.250
medial	high	male	1	3	3.011
medial	high	male	1	3	2.241
medial	high	male	2	1	2.081
medial	high	male	2	2	1.492
medial	high	male	2	3	0.608
medial	high	male	2	3	1.817
medial	high	male	5	1	0.844
medial	high	male	5	1	0.803
medial	high	male	5	2	2.269
medial	high	male	5	2	1.612
medial	high	male	5	3	2.175
medial	high	male	5	3	1.287
medial	high	male	8	1	0.870
medial	high	male	8	1	0.036
medial	high	male	8	3	2.689
medial	high	male	8	3	1.168

Table A.2. Values of head thermal insulation ($I_{t,head}$) and evaporative resistance ($R_{et,head}$) with different types of headgear under varying air velocities (v_a) obtained from measurements with manikins or head forms presented in Figures and Tables of the cited references (na: data not available).

Reference	Source	Helmet type	Description	v_a ($m \cdot s^{-1}$)	$I_{t,head}$ ($m^2 \cdot K \cdot W^{-1}$)	$R_{et,head}$ ($m^2 \cdot Pa \cdot W^{-1}$)
Aljaste et al., 2015	Fig5/ Fig8	Bicycle	Etto-Bic	1.60	0.049	na
		Bicycle	H5-Bic	1.60	0.045	11.486
	Fig6/ Fig9	Bicycle	HA12	1.60	0.047	11.216
		Bicycle	HA13	1.60	0.049	11.486
		Bicycle	Etto-Wig	1.60	0.088	15.709
		Bicycle	H5-Wig	1.60	0.085	16.471
		Bicycle	HA12-Wig	1.60	0.077	18.824
	Fig7	Bicycle	HA13-Wig	1.60	0.077	18.408
		Bicycle	H5-Wig	6.00	0.045	na
		Bicycle	HA12-Wig	6.00	0.046	na
Chen et al., 2006	Tab2/4	Bicycle	HA13-Wig	6.00	0.047	na
		Military	MilitaryHorPad	0.05	0.232	72.800
		Military	MilitarySuspens	0.05	0.204	68.950
Fonseca, 1974	Tab1	Military	MilitaryVertPad	0.05	0.227	74.350
		Military	Hayes-Stewart-H	0.10	0.174	19.129
		Military	Hayes-Stewart-H	2.00	0.082	7.779
		Military	Hayes-Stewart-H	5.00	0.065	3.945
		Military	Helmet/Ventilat	0.10	0.141	18.997
		Military	Helmet/Ventilat	2.00	0.076	7.192
		Military	Helmet/Ventilat	5.00	0.059	3.570
	Tab2	Military	Tankers Helmet	0.10	0.231	55.988
		Military	Tankers Helmet	0.10	0.226	52.751
		Military	Tankers Helmet	3.00	0.135	13.621
		Military	Tankers Helmet	3.00	0.129	12.183
	Tab3	Military	Helmet1	0.10	0.136	28.506
		Military	Helmet1	3.00	0.065	8.577
		Military	Helmet2	0.10	0.167	28.182
		Military	Helmet2	3.00	0.073	4.697
		Military	Helmet3	0.10	0.166	23.376
		Military	Helmet3	3.00	0.064	4.097
		Military	Helmet4	0.10	0.163	21.443
		Military	Helmet4	3.00	0.060	4.071
		Military	Helmet5	0.10	0.155	21.350
		Military	Helmet5	3.00	0.057	4.089
	Tab4	Military	M-1 open slots	0.10	0.146	16.981
		Military	M-1 open slots	3.00	0.056	4.281
		Military	M-1 sealed slot	0.10	0.160	23.038
		Military	M-1 sealed slot	3.00	0.056	4.450
	Tab5	Military	Head area 47%	0.10	0.149	19.605
		Military	Head area 47%	3.00	0.050	3.904
		Military	Head area 54%	0.10	0.155	21.846
		Military	Head area 54%	3.00	0.050	4.062
		Military	Head area 60%	0.10	0.160	23.038
		Military	Head area 60%	3.00	0.054	4.697
	Tab7	Military	Head area 67%	0.10	0.166	23.376
		Military	Head area 67%	3.00	0.064	4.097
		Military	M-1 susp HEL	0.10	0.171	24.603
		Military	M-1 susp HEL	3.00	0.064	4.097

Reference	Source	Helmet type	Description	V_a ($m \cdot s^{-1}$)	$I_{t,head}$ ($m^2 \cdot K \cdot W^{-1}$)	$R_{et,head}$ ($m^2 \cdot Pa \cdot W^{-1}$)
		Military	M-1 susp HEL	3.00	0.060	5.234
		Military	M-1 susp Std	0.10	0.171	23.485
		Military	M-1 susp Std	3.00	0.060	4.697
		Military	M-1 Welson	0.10	0.161	23.829
		Military	M-1 Welson	3.00	0.059	4.958
	Tab8	Military	M-1 shield down	0.10	0.186	24.506
		Military	M-1 shield down	3.00	0.081	5.551
		Military	M-1 shield up	0.10	0.167	22.055
		Military	M-1 shield up	3.00	0.068	4.921
		Military	Riot shield dow	0.10	0.222	28.582
		Military	Riot shield dow	3.00	0.084	6.263
		Military	Riot shield up	0.10	0.209	24.866
		Military	Riot shield up	3.00	0.078	4.697
	Tab9	Military	AirAFH1	0.10	0.267	24.858
		Military	AirAFH1	3.00	0.074	5.124
		Military	AirAFH5	0.10	0.225	28.981
		Military	AirAFH5	3.00	0.079	6.654
		Military	CVC	0.10	0.198	26.140
		Military	CVC	3.00	0.067	4.867
		Military	EngMilitary	0.10	0.150	20.709
		Military	EngMilitary	3.00	0.057	4.965
		Military	Football	0.10	0.180	29.451
		Military	Football	3.00	0.073	5.660
		Military	Hayes-Stewart-E	0.10	0.172	26.737
		Military	Hayes-Stewart-E	3.00	0.070	4.859
		Military	ItalMilitary	0.10	0.160	21.990
		Military	ItalMilitary	3.00	0.065	4.697
		Military	Parachutist	0.10	0.211	25.552
		Military	Parachutist	3.00	0.084	6.263
Kuklane et al., 2015	Fig10	Bicycle	Etto-Wig	1.60	0.102	na
		Bicycle	KK-Wig	1.60	0.089	na
		Bicycle	RP-Wig	1.60	0.087	na
		Bicycle	TS-Wig	1.60	0.092	na
	Fig11	Bicycle	Etto-Wig	6.00	0.046	na
		Bicycle	KK-Wig	6.00	0.044	na
		Bicycle	RP-Wig	6.00	0.036	na
		Bicycle	TS-Wig	6.00	0.044	na
	Fig8	Bicycle	Etto-Bic	0.20	0.167	na
		Bicycle	KK	0.20	0.139	na
		Bicycle	RP	0.20	0.139	na
		Bicycle	TS	0.20	0.166	na
	Fig9/ Fig13	Bicycle	Etto-Bic	1.60	0.059	14.456
		Bicycle	H17-Bic	1.60	0.056	12.016
		Bicycle	H20-Bic	1.60	0.060	12.865
		Bicycle	H5-Bic	1.60	0.055	11.751
		Bicycle	KK	1.60	0.056	na
		Bicycle	RP	1.60	0.050	na
		Bicycle	TS	1.60	0.055	na
Liu and Holmér, 1995	Tab1	Industrial	Helmet1	0.10	na	44.000
		Industrial	Helmet2	0.10	na	42.000

Reference	Source	Helmet type	Description	V_a ($m \cdot s^{-1}$)	$I_{t,head}$ ($m^2 \cdot K \cdot W^{-1}$)	$R_{et,head}$ ($m^2 \cdot Pa \cdot W^{-1}$)
		Industrial	Helmet3	0.10	na	47.000
		Industrial	Helmet4	0.10	na	38.000
		Industrial	Helmet5	0.10	na	38.000
Liu and Holmér, 1997	Fig4	Industrial	Helmet1	0.10	na	22.705
		Industrial	Helmet1	0.40	na	15.984
		Industrial	Helmet2	0.10	na	21.718
		Industrial	Helmet2	0.40	na	15.137
		Industrial	Helmet3	0.10	na	27.184
		Industrial	Helmet3	0.40	na	20.285
		Industrial	Helmet4	0.10	na	20.598
		Industrial	Helmet4	0.40	na	14.584
		Industrial	Helmet5	0.10	na	21.600
		Industrial	Helmet5	0.40	na	14.071
		Industrial	Helmet6	0.10	na	33.865
		Industrial	Helmet6	0.40	na	17.374
		Bicycle	Helmet7	0.10	na	27.370
		Bicycle	Helmet7	0.40	na	18.164
	Fig5	Industrial	Helmet1	0.10	na	23.356
		Industrial	Helmet1	0.40	na	17.793
		Industrial	Helmet2	0.10	na	23.994
		Industrial	Helmet2	0.40	na	17.296
		Industrial	Helmet3	0.10	na	29.018
		Industrial	Helmet3	0.40	na	20.694
		Industrial	Helmet4	0.10	na	22.222
		Industrial	Helmet4	0.40	na	17.044
		Industrial	Helmet5	0.10	na	23.304
		Industrial	Helmet5	0.40	na	17.017
		Industrial	Helmet6	0.10	na	33.869
		Industrial	Helmet6	0.40	na	18.676
		Bicycle	Helmet7	0.10	na	29.755
		Bicycle	Helmet7	0.40	na	19.363
Martinez, 2016	Fig2.10b	Bicycle	Tilted-2z-Bicycle1	1.60	0.103	na
		Bicycle	Tilted-2z-Bicycle2	1.60	0.095	na
		Bicycle	Tilted-2z-Bicycle3	1.60	0.088	na
		Bicycle	Tilted-2z-Bicycle4	1.60	0.089	na
		Bicycle	Tilted-2z-Bicycle5	1.60	0.080	na
		Bicycle	Tilted-2z-Bicycle6	1.60	0.077	na
		Bicycle	Tilted-2z-Bicycle1	6.10	0.058	na
		Bicycle	Tilted-2z-Bicycle2	6.10	0.054	na
		Bicycle	Tilted-2z-Bicycle3	6.10	0.050	na
		Bicycle	Tilted-2z-Bicycle4	6.10	0.048	na
		Bicycle	Tilted-2z-Bicycle5	6.10	0.044	na
		Bicycle	Tilted-2z-Bicycle6	6.10	0.045	na
		Bicycle	Tilted-9z-Bicycle1	1.60	0.112	na
		Bicycle	Tilted-9z-Bicycle2	1.60	0.102	na
		Bicycle	Tilted-9z-Bicycle3	1.60	0.099	na
		Bicycle	Tilted-9z-Bicycle4	1.60	0.087	na
		Bicycle	Tilted-9z-Bicycle5	1.60	0.087	na
		Bicycle	Tilted-9z-Bicycle6	1.60	0.081	na
		Bicycle	Tilted-9z-Bicycle1	6.10	0.059	na

Reference	Source	Helmet type	Description	V_a ($m \cdot s^{-1}$)	$I_{t,head}$ ($m^2 \cdot K \cdot W^{-1}$)	$R_{et,head}$ ($m^2 \cdot Pa \cdot W^{-1}$)
		Bicycle	Tilted-9z-Bicycle2	6.10	0.057	na
		Bicycle	Tilted-9z-Bicycle3	6.10	0.049	na
		Bicycle	Tilted-9z-Bicycle4	6.10	0.051	na
		Bicycle	Tilted-9z-Bicycle5	6.10	0.047	na
		Bicycle	Tilted-9z-Bicycle6	6.10	0.044	na
		Bicycle	Upright-2z-Bicycle1	1.60	0.111	na
		Bicycle	Upright-2z-Bicycle2	1.60	0.108	na
		Bicycle	Upright-2z-Bicycle3	1.60	0.102	na
		Bicycle	Upright-2z-Bicycle4	1.60	0.090	na
		Bicycle	Upright-2z-Bicycle5	1.60	0.095	na
		Bicycle	Upright-2z-Bicycle6	1.60	0.089	na
		Bicycle	Upright-2z-Bicycle1	6.10	0.059	na
		Bicycle	Upright-2z-Bicycle2	6.10	0.056	na
		Bicycle	Upright-2z-Bicycle3	6.10	0.054	na
		Bicycle	Upright-2z-Bicycle4	6.10	0.051	na
		Bicycle	Upright-2z-Bicycle5	6.10	0.047	na
		Bicycle	Upright-2z-Bicycle6	6.10	0.048	na
		Bicycle	Upright-9z-Bicycle1	1.60	0.114	na
		Bicycle	Upright-9z-Bicycle2	1.60	0.121	na
		Bicycle	Upright-9z-Bicycle3	1.60	0.115	na
		Bicycle	Upright-9z-Bicycle4	1.60	0.107	na
		Bicycle	Upright-9z-Bicycle5	1.60	0.100	na
		Bicycle	Upright-9z-Bicycle6	1.60	0.094	na
		Bicycle	Upright-9z-Bicycle1	6.10	0.062	na
		Bicycle	Upright-9z-Bicycle2	6.10	0.064	na
		Bicycle	Upright-9z-Bicycle3	6.10	0.062	na
		Bicycle	Upright-9z-Bicycle4	6.10	0.055	na
		Bicycle	Upright-9z-Bicycle5	6.10	0.057	na
		Bicycle	Upright-9z-Bicycle6	6.10	0.052	na
	Mukunthan et al., 2019	Bicycle	A1	3.00	0.051	na
		Bicycle	A1	6.00	0.046	na
		Bicycle	A2	3.00	0.069	na
		Bicycle	A2	6.00	0.055	na
		Bicycle	A3	3.00	0.057	na
		Bicycle	A3	6.00	0.049	na
		Bicycle	A4	3.00	0.054	na
		Bicycle	A4	6.00	0.047	na
		Bicycle	H1	3.00	0.058	na
		Bicycle	H1	6.00	0.048	na
	Pang et al., 2014	Cricket	Elite-Cricket	0.08	0.159	36.220
		Cricket	Masu-Cricket	0.08	0.187	60.160
		Cricket	NXT-Cricket	0.08	0.171	55.720
		Cricket	Prem-Cricket	0.08	0.172	44.720
		Cricket	Ulti-Cricket	0.08	0.169	44.490
	Ueno and Sawada, 2019	Industrial	A	1.00	na	13.984
		Industrial	A	1.00	na	13.238
		Industrial	A	2.00	na	9.640
		Industrial	A	2.00	na	9.279
		Industrial	A	3.00	na	7.465
		Industrial	A	3.00	na	7.579

Reference	Source	Helmet type	Description	V_a ($m \cdot s^{-1}$)	$I_{t,head}$ ($m^2 \cdot K \cdot W^{-1}$)	$R_{et,head}$ ($m^2 \cdot Pa \cdot W^{-1}$)
		Industrial	AS	1.00	na	14.819
		Industrial	AS	1.00	na	13.238
		Industrial	AS	2.00	na	10.029
		Industrial	AS	2.00	na	9.109
		Industrial	AS	3.00	na	7.355
		Industrial	AS	3.00	na	7.355
		Industrial	AS_O	1.00	na	15.760
		Industrial	AS_O	1.00	na	13.601
		Industrial	AS_O	2.00	na	9.734
		Industrial	AS_O	2.00	na	9.547
		Industrial	AS_O	3.00	na	8.007
		Industrial	AS_O	3.00	na	7.465
		Industrial	AS_O_S	1.00	na	13.790
		Industrial	AS_O_S	1.00	na	13.417
		Industrial	AS_O_S	2.00	na	9.367
		Industrial	AS_O_S	2.00	na	9.456
		Industrial	AS_O_S	3.00	na	7.638
		Industrial	AS_O_S	3.00	na	7.638
		Industrial	AS_S	1.00	na	13.238
		Industrial	AS_S	1.00	na	13.238
		Industrial	AS_S	2.00	na	9.456
		Industrial	AS_S	2.00	na	9.026
		Industrial	AS_S	3.00	na	7.247
		Industrial	AS_S	3.00	na	7.195
		Industrial	A_O	1.00	na	14.819
		Industrial	A_O	1.00	na	13.601
		Industrial	A_O	2.00	na	9.929
		Industrial	A_O	2.00	na	9.367
		Industrial	A_O	3.00	na	7.579
		Industrial	A_O	3.00	na	7.410
		Industrial	B	1.00	na	13.601
		Industrial	B	1.00	na	12.895
		Industrial	B	2.00	na	9.193
		Industrial	B	2.00	na	8.865
		Industrial	B	3.00	na	7.522
		Industrial	B	3.00	na	7.301
Zwolinska et al., 2014	Fig4	Military	Ballistic-A	0.45	0.135	na
		Military	Ballistic-B	0.45	0.150	na
		Military	Ballistic-C	0.45	0.130	na
		Military	Ballistic-D	0.45	0.123	na

Table A.3. Values of head level boundary air layer thermal insulation ($I_{a,head}$) and evaporative resistance ($R_{ea,head}$) under varying air velocities (v_a) obtained from measurements with nude manikins or head forms presented in Figures and Tables of the cited references (na: data not available).

Reference	Source	Helmet type	Description	v_a ($m \cdot s^{-1}$)	$I_{a,head}$ ($m^2 \cdot K \cdot W^{-1}$)	$R_{ea,head}$ ($m^2 \cdot Pa \cdot W^{-1}$)
Aljaste et al., 2015	Fig5/Fig8	nude	nude	1.60	0.042	10.608
	Fig6/Fig9	nude	nude-Wig	1.60	0.070	15.087
Brühwiler, 2003	Fig3	nude	nude	0.12	0.141	na
		nude	nude	1.00	0.063	na
		nude	nude	2.00	0.048	na
		nude	nude	3.00	0.040	na
		nude	nude	4.00	0.034	na
		nude	nude	5.00	0.031	na
		nude	nude	6.00	0.028	na
Fonseca, 1974	Tab1	nude	nude	0.10	0.099	9.697
		nude	nude	2.00	0.067	5.940
		nude	nude	5.00	0.051	3.100
Kuklane et al., 2015	Fig10	nude	nude-Wig	1.60	0.077	na
	Fig8	nude	nude	0.20	0.103	na
	Fig9/Fig13	nude	nude	1.60	0.047	11.273
Liu and Holmér, 1995	Tab1	nude	nude	0.10	na	28.000
Lu et al., 2015	Tab6	nude	nude	0.15	0.102	na
		nude	nude	1.55	0.052	na
		nude	nude	4.00	0.032	na
Martinez, 2016	Tab3.2	nude	nude	0.09	0.108	na
Mukunthan et al., 2019	Tab.3	nude	nude	3.00	0.052	na
		nude	nude	6.00	0.046	na
Pang et al., 2014	Tab1/2	nude	nude	0.08	0.105	45.760
Psikuta et al., 2016	Tab.2	nude	nude-Diana	0.10	0.094	na
		nude	nude-Newton	0.10	0.116	na
		nude	nude-Sam	0.10	0.091	na
		nude	nude-Tore	0.10	0.182	na
Ueno and Sawada, 2019	Fig3d(IV)	nude	nude	1.00	na	10.563
		nude	nude	1.00	na	10.343
		nude	nude	2.00	na	7.092
		nude	nude	2.00	na	7.143
		nude	nude	3.00	na	5.739
		nude	nude	3.00	na	5.773
Wang et al., 2012	Fig2	nude	nude	0.18	na	33.866
		nude	nude	0.18	na	32.894
		nude	nude	0.48	na	17.500
		nude	nude	0.48	na	18.850
		nude	nude	0.78	na	8.318
		nude	nude	0.78	na	8.966
Zwolinska et al., 2014	Fig4	nude	nude	0.45	0.094	na

Figure 1

Click here to
access/download:Figure, Fig1.pdf

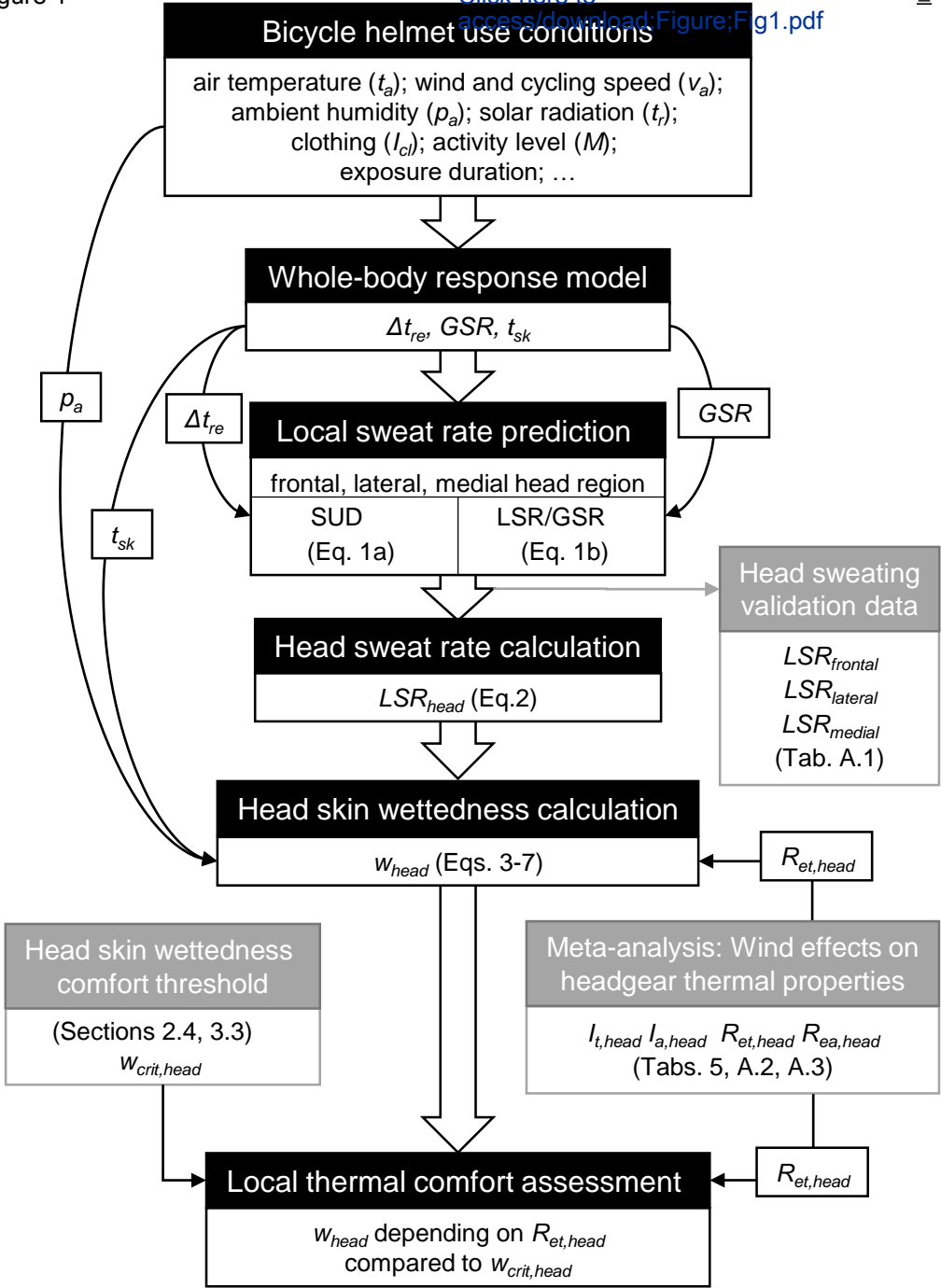
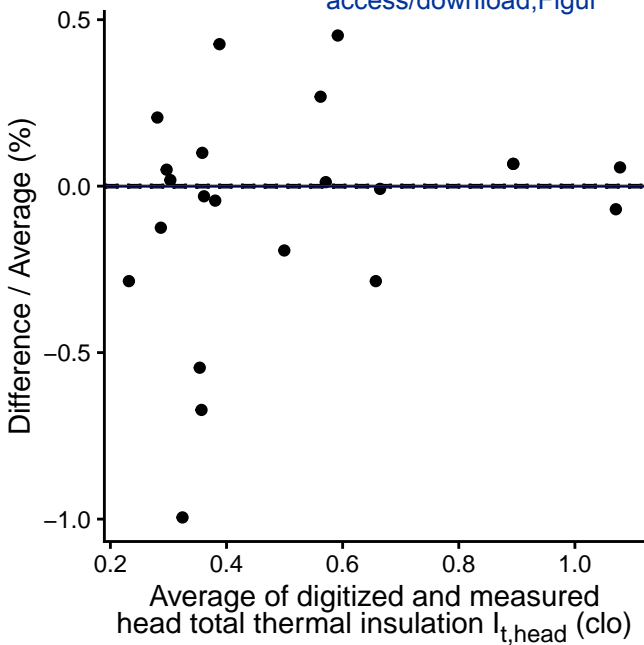


Figure 2

[Click here to
access/download;Figur](#)



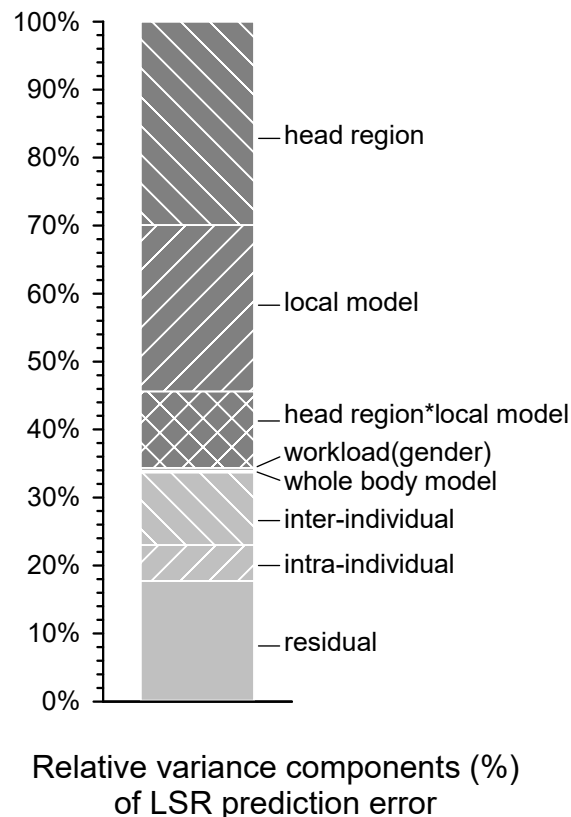
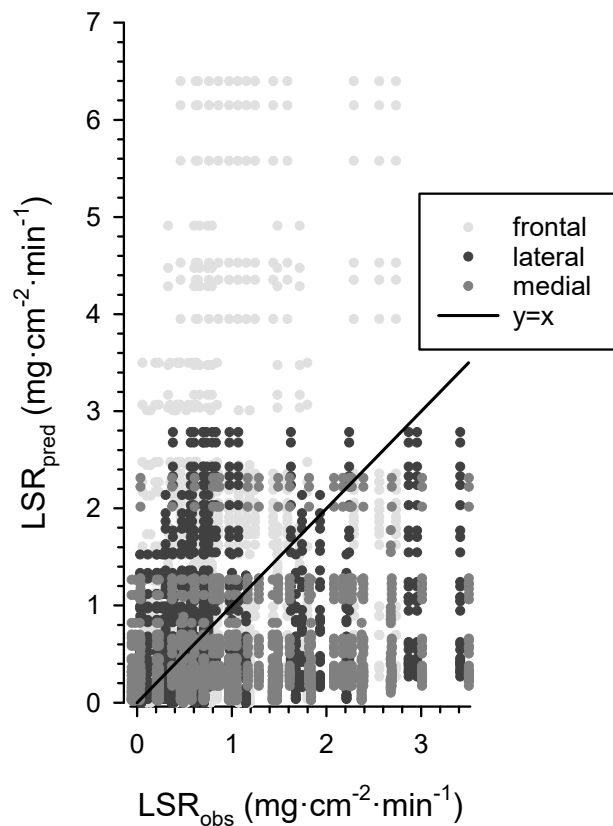


Figure 4

[Click here to access/download;Figure;Fig4.PDF](#)

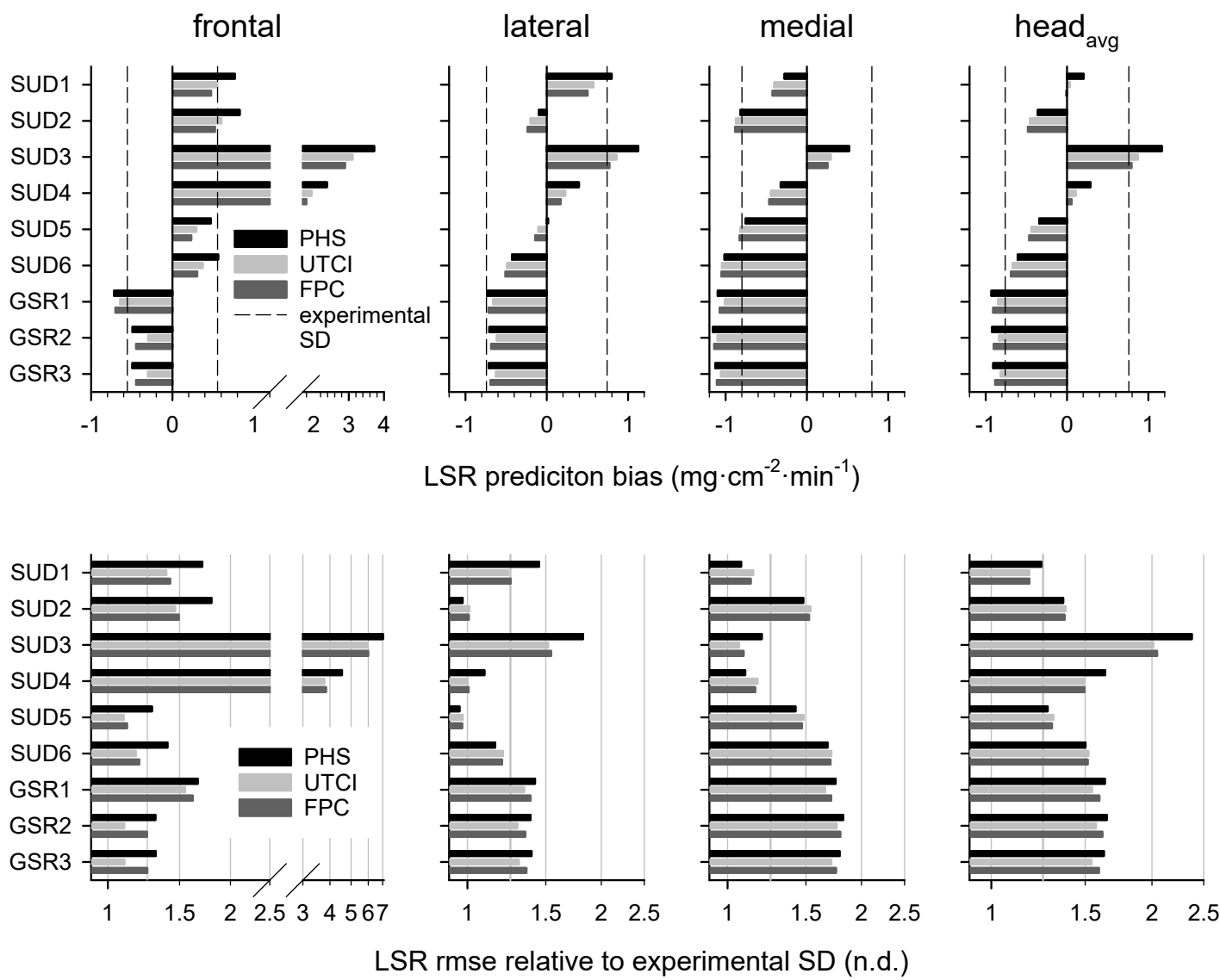
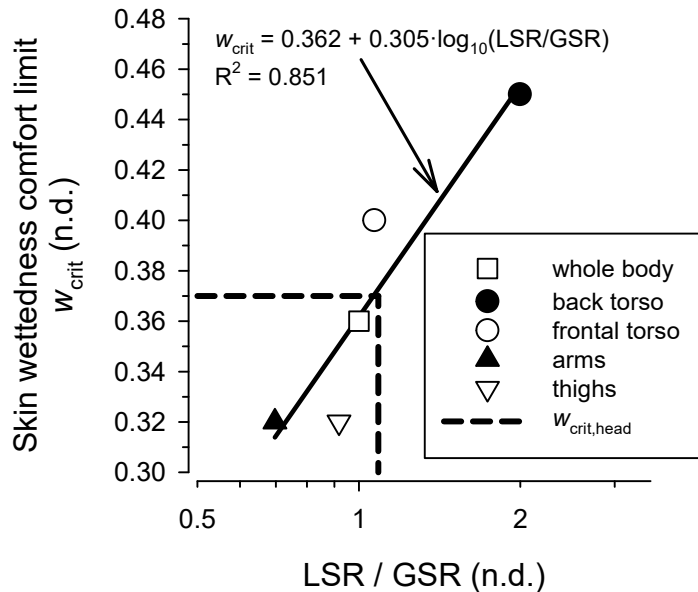
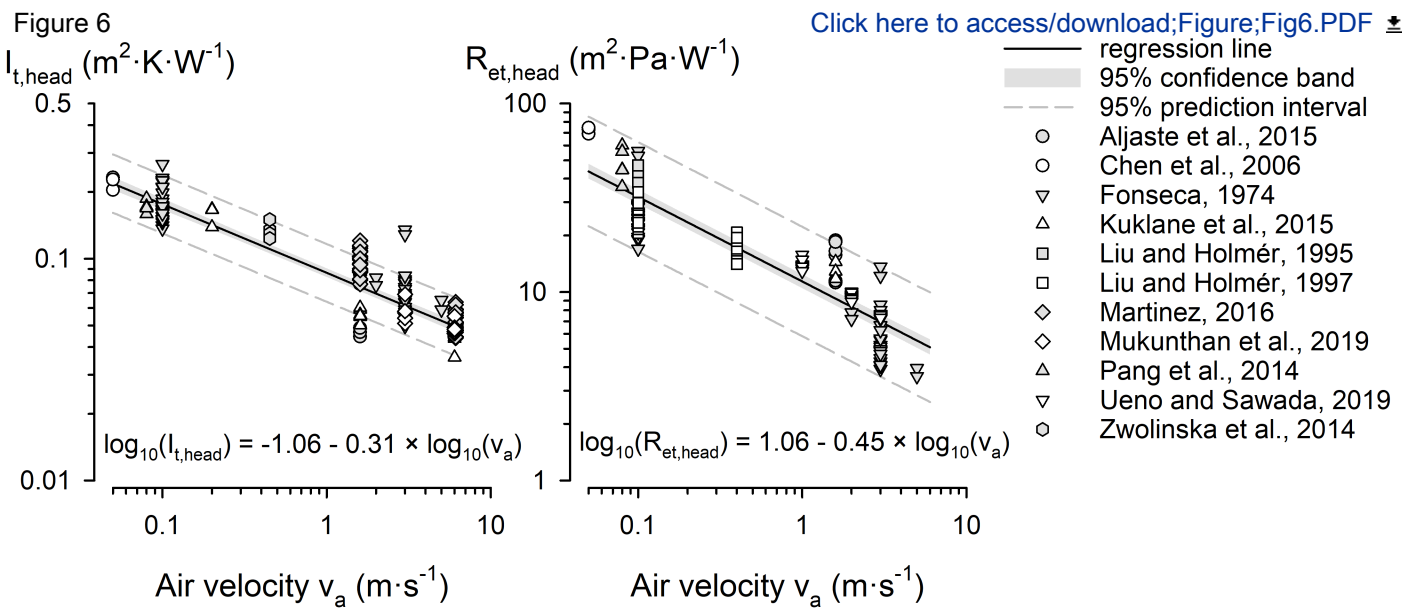


Figure 5

[Click here to access/download;Figure;](#)





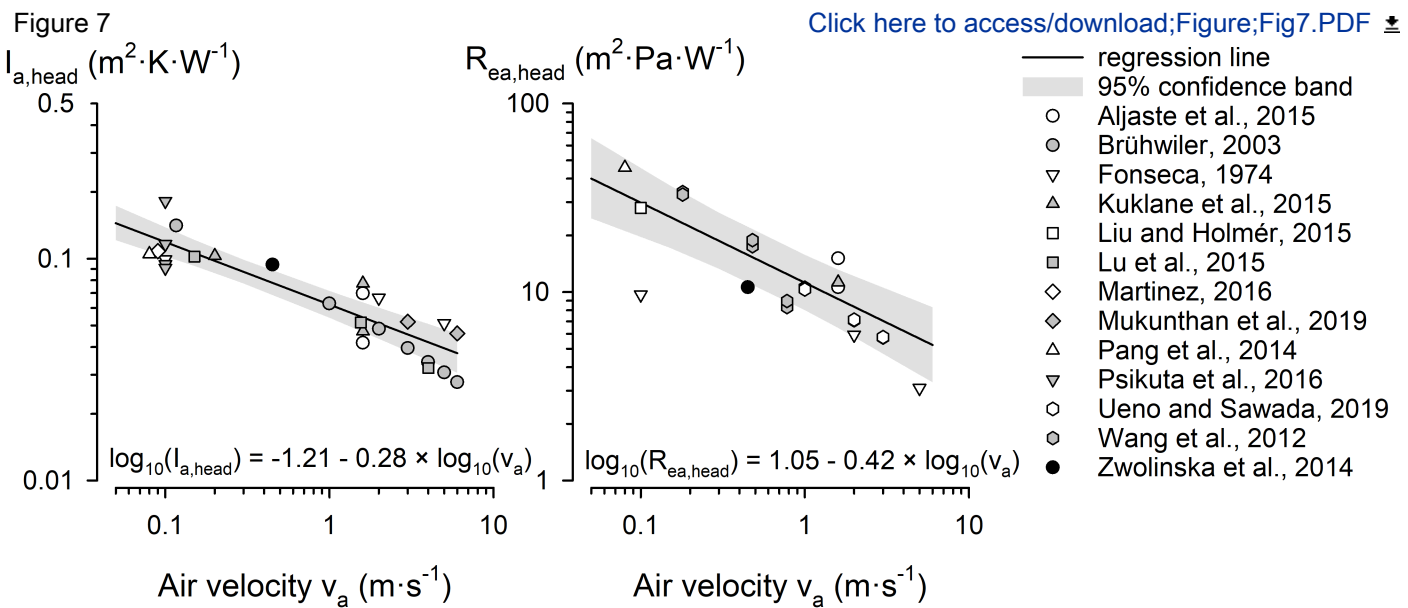
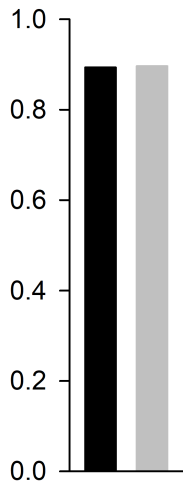
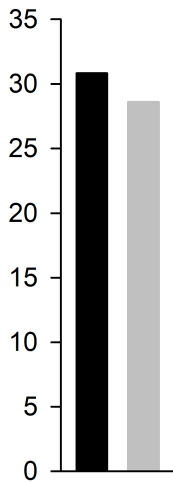


Figure 8

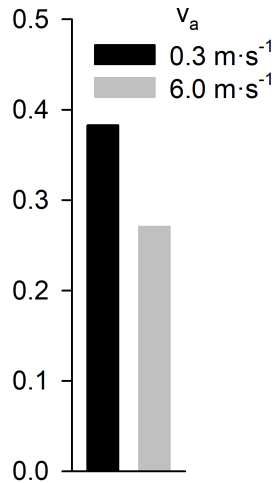
Δt_{re}
(°C)



t_{sk}
(°C)



GSR
(mg·cm⁻²·min⁻¹)



w_{head} (n.d.)

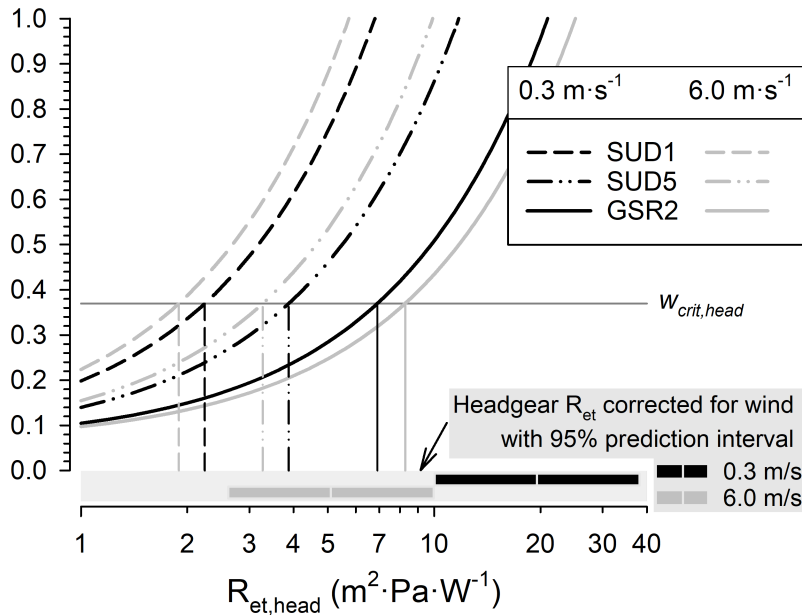


Figure captions

Figure 1. Elements of the proposed modelling framework for local thermal comfort assessment under bicycle helmet use conditions. From top to bottom, the flowchart depicts the modelling steps with references to input and output variables (cf. list of abbreviations) and governing equations, tables and supplemental information. Grey shaded boxes indicate the supplemental analyses concerning the validation data on head perspiration, the meta-analysis on wind effect on headgear thermal properties, and the derivation of a skin wettedness comfort threshold for the head region, respectively.

Figure 2. Percentage deviations between digitized and measured values of head total thermal insulation ($I_{t,head}$) in clo units ($1 \text{ clo} = 0.155 \text{ m}^2 \cdot \text{K} \cdot \text{W}^{-1}$) from the measurements reported by Kuklane et al. (2015), cf. Tables A.2 & A.3, with the dashed horizontal line indicating median bias.

Figure 3. (a) Twenty-seven (3 whole-body models \times 9 local models) predictions of local sweat rates (LSR_{pred}) for each condition at the frontal, lateral and medial head regions compared to the corresponding observed values (LSR_{obs}) from Table A.1. (b) Results of the variance component analysis with a decomposition of the LSR prediction error ($=LSR_{pred} - LSR_{obs}$) indicating the relative influence of the head region, the local models and their interaction, as well as of the workload conditions and whole-body models compared to the inter-individual, intra-individual and residual variance (the latter including all other two-way and higher-order interaction terms).

Figure 4. Mean LSR prediction error (bias, upper panel) with positive values indicating overestimation and negative values indicating underestimation of measured LSR compared to the experimental SD (vertical reference lines), and root-mean-squared error (rmse, lower panel). Data were pooled for the low and high workload conditions (Eq. 8). Calculations were performed with nine local models (Table 2) coupled with the whole-body models PHS, UTCI-Fiala and FPC, respectively, for the frontal, lateral and medial regions. Statistics for the covered head area ($head_{avg}$) were computed from the regional prediction errors as area-weighted average using the weighing scheme from Eq. 2.

Figure 5. Regression of skin wettedness comfort limits (w_{crit}) for various body parts (Fukazawa and Havenith, 2009) on sweating sensitivity (GSR2 from Table 1) with derived $w_{crit,head}$.

Figure 6. Meta-analysis of the effect of air velocity (v_a) on headgear's total thermal insulation ($I_{t,head}$, left panel), and evaporative resistance ($R_{et,head}$, right panel) presenting log-log-linear regression equations with 95% confidence bands for the regression lines as derived from published measurements with varying headgear using random coefficient mixed models.

Figure 7. Meta-analysis of the effect of air velocity (v_a) on boundary air layer thermal insulation ($I_{a,head}$, left panel), and evaporative resistance ($R_{ea,head}$, right panel) at uncovered head level. Log-log-linear regression equations with 95% confidence bands for the regression lines were derived from published measurements with nude manikins or head forms using random coefficient mixed models.

Figure 8. Core temperature increase (Δt_{re}), mean skin temperature (t_{sk}) and whole body gross sweat rate (GSR) predicted by the UTCI-Fiala model for the commuter cycling scenario with low and high relative air velocities (v_a), and resulting head skin wettedness (w_{head}) in relation to headgear evaporative resistance ($R_{et,head}$). Vertical reference lines indicate the upper limit of $R_{et,head}$ for maintaining w_{head} below the skin wettedness comfort limit $w_{crit,head}$. Corrections for the effect of v_a on $R_{et,head}$ with 95% prediction intervals were calculated as in Figure 6 using the regression coefficients from Table 5.

Tables

Table 1. Sources with references to the literature and descriptions of models predicting local sweat rates (LSR) at the head via sudomotor sensitivities (*SUD*) and as the ratio of *LSR* to gross sweat rate (*GSR*), respectively.

Identifier	Source	Description of conditions
SUD1	Ref1	45 min incremental cycling protocol (50-100 W) in the heat (n=10)
SUD2	Ref2	30 min treadmill running at 55% VO_{2max} @25°C, n=9 (frontal), n=4 (lateral, medial head)
SUD3	Ref2	30 min running at 75% VO_{2max} subsequent to SUD2
SUD4	Ref2	Overall results from combined SUD2 & SUD3 protocol
SUD5	Ref3	Cycling in the heat at 125 W (n=46)
SUD6	Ref3	Resting in the heat (n=49)
GSR1	Ref3	LSR set equal to GSR
GSR2	Ref2	Conditions identical to SUD2
GSR3	Ref2	Conditions identical to SUD3

Notes: Ref1: Machado-Moreira et al. (2008b); Ref2: Smith and Havenith (2011); Ref3: Taylor and Machado-Moreira (2013); n: sample size in experiments underlying the parameter; VO_{2max} : maximum oxygen uptake

Table 2. Coefficients for predicting local sweat rates (LSR) at the frontal, lateral and medial head regions via sudomotor sensitivities (*SUD*) and as the ratio of LSR to gross sweat rate (*GSR*), respectively (n.d.: non-dimensional).

Identifier	Head region		
	frontal	lateral	medial
Sudomotor sensitivity ($mg \cdot cm^{-2} \cdot min^{-1} \cdot ^\circ C^{-1}$)			
SUD1	1.89	1.93	1.06
SUD2	1.96	0.90	0.48
SUD3	5.31	2.31	1.92
SUD4	3.76	1.47	1.01
SUD5	1.55	1.03	0.55
SUD6	1.65	0.52	0.27
LSR / GSR ratio (n.d.)			
GSR1	1	1	1
GSR2	2.61	1.20	0.64
GSR3	2.60	1.16	0.81

Table 3. Summary statistics for the data from Table A.1 with the number of measurements (n), means, standard deviations (SD), minimum (Min) and maximum (Max) values of local sweat rates observed (*LSR_{obs}*) at the frontal (forehead), lateral (temple) and medial head regions under low and high workload conditions (De Bruyne et al., 2008).

Workload	Head region	n	<i>LSR_{obs}</i> ($mg \cdot cm^{-2} \cdot min^{-1}$)			
			Mean	SD	Min	Max
low	frontal	22	0.56	0.40	0.06	1.80
	lateral	23	0.56	0.53	0.03	2.21
	medial	20	0.78	0.64	-0.06	2.37
high	frontal	21	1.18	0.68	0.33	2.73
	lateral	23	1.20	0.90	0.30	3.41
	medial	21	1.72	0.93	0.04	3.51

Table 4. Core temperature increase (Δt_{re}) and gross sweat rate (GSR) predicted by the whole-body models PHS, UTCI-Fiala and FPC, respectively, at the end of the cycling periods for the gender-specific workload conditions with specified power output (De Bruyne et al., 2008) assuming 20% gross cycling efficiency. Note that FPC predicted zero sweating for the 80 W (low-female) power output setting.

<i>Workload</i>	<i>Gender / Power output</i>	Δt_{re} (°C)			<i>GSR</i> (mg·cm ⁻² ·min ⁻¹)		
		<i>PHS</i>	<i>UTCI</i>	<i>FPC</i>	<i>PHS</i>	<i>UTCI</i>	<i>FPC</i>
low	female / 80 W	0.57	0.46	0.29	0.038	0.061	0.000
	male / 100 W	0.66	0.58	0.43	0.064	0.128	0.035
high	female / 120 W	0.92	0.81	0.84	0.156	0.234	0.214
	male / 150 W	1.20	1.05	1.16	0.266	0.379	0.343

Table 5. Regression results for the effects of air velocity (v_a) on headgear thermal insulation ($I_{t,head}$) and evaporative resistance ($R_{et,head}$) as well as on head boundary air layer thermal insulation ($I_{a,head}$) and evaporative resistance ($R_{ea,head}$). Estimates of intercept (α) and slope (β) with standard errors (SE) and P-values were obtained by fitting log-log-linear regression functions $\log_{10} y = \alpha + \beta \times \log_{10} v_a$ to the data from Table A.2 and Table A.3.

<i>y</i>	α (SE)	$P_{ \alpha=0}$	β (SE)	$P_{ \beta=0}$
$I_{t,head}$	-1.06 (0.01)	<.0001	-0.31 (0.01)	<.0001
$R_{et,head}$	1.06 (0.02)	<.0001	-0.45 (0.01)	<.0001
$I_{a,head}$	-1.21 (0.03)	<.0001	-0.28 (0.03)	<.0001
$R_{ea,head}$	1.05 (0.06)	<.0001	-0.42 (0.07)	<.0001